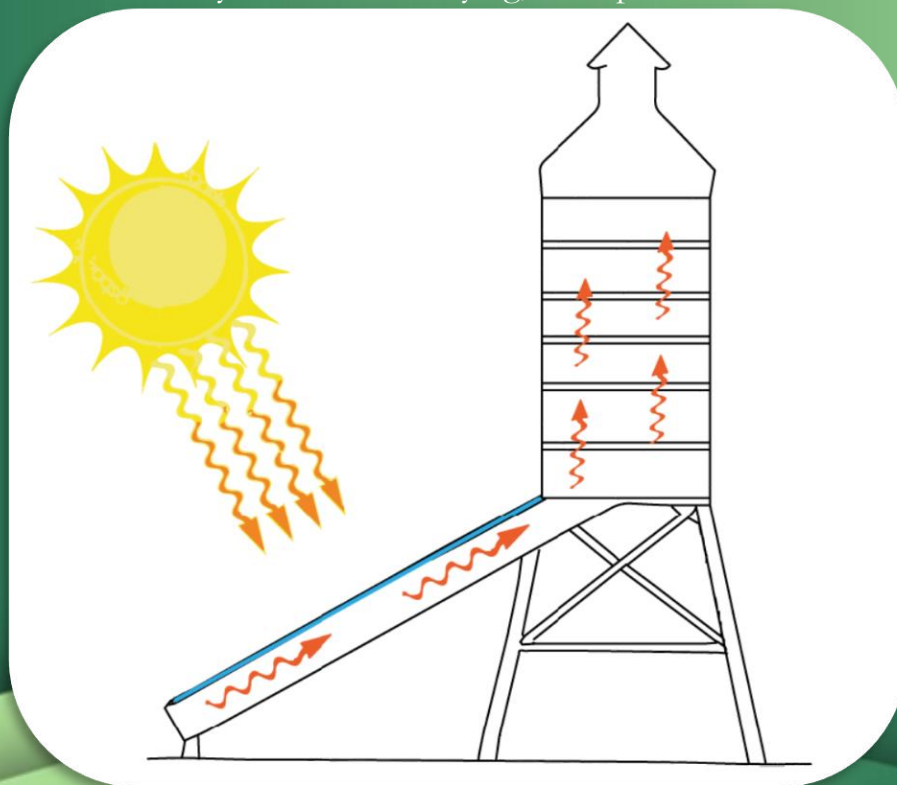# Modelling of a solar dryer for food preservation in developing countries

Joakim Olsson
2016-06-27
Key words: Solar drying, food preservation

Abstract

Food insecurity has proven to be a significant problem in many developing countries, which in some cases occurs due to the lack of adequate methods of preserving foods for longer periods of time. Solar drying of foods could be a feasible method for preserving foods in developing countries. To maintain a good product quality, the design of the solar dryer used needs to be considered. A faulty design will result in the foods being exposed to either excessive heat, which will degrade nutrients such as Vitamin C, or exposed to insufficient heat which could result in growth of mold or bacteria.

In this study a base scenario for a solar dryer design has been set up and mathematically analysed to find ways of improving the design and identifying the most important parameters to consider. The study will serve as a part of an ongoing project at Lund University in Sweden, which will be implemented Mozambique. The results of the study imply that the collector performance can be improved significantly if the most important parameters are optimized. For future work, more practical measurements would be required to verify the results, particularly regarding the evaporation rate of the drying products.

Summary

The malnutrition in developing countries has proven to be a persistent problem over the decades and appears to remain unsolved despite the economic growth that has occurred in some of the countries. Among these developing countries is Mozambique, which had a Human Development Index (HDI) positioned at rank 180 out of 188 countries and territories in 2014 by the United Nations Developing Programme. Almost one-third of Mozambicans, most of them living in the south and centre regions, suffer from chronic food insecurity and the country is prone and sensitive to natural disasters such as drought and flooding. This food insecurity could be counteracted by the fact that the annual fruit and crop harvests provide an abundance of food during the harvest seasons, but food preservation methods are currently inadequate. However, Mozambique has over the last few decades undergone significant economic development, opening up new opportunities to solve this problem.

One method to reduce the food insecurity of Mozambique would be to find a simple and cheap way of preserving the abundant foods of the harvest season, which is the aim of an on-going project at Lund University. The idea is to use semi-permeable bags that can hold fruit juices combined with solar dryers to dry out the bags more efficiently. This will preserve the nutrients of the fruits while the product is protected from external exposure.

The aim of this report is to present a theoretical model of a solar collector connected to a drying tower holding SAP-pouches in order to estimate if the generated temperatures are sufficient to maintain a good product quality. The model built in Maple 2015, a software used for analysing and solving mathematical problems, uses relevant equations for heat- and mass transfer and can be used as a method of generating approximate temperatures and the drying rate of an indirect solar dryer. The mathematical model covers a solar collector and a drying tower, where the collector has a rectangular cross-section and consists of a single glass layer, an absorber, a constant air flow and thermal insulation on the sides and bottom. The dryer, also with a rectangular cross-section area, will consist of a tower with side insulation and shelves to place the SAP-pouches on as well as a constant upward air flow. The model includes the effects of relative humidity, variable heat transfer coefficients for radiation and convection, ambient temperature, solar irradiation as well as the properties and dimensions of the materials used for all components.

The model resulted in a simple and flexible calculation tool that can be used to generate approximate values for the collector and dryer temperatures, granting the user relevant information of the overall dryer performance for the selected materials and dimensions. The results are implying that the solar dryer performance can be improved significantly through optimization of various parameters. The main assumption made is for the radiation model of the absorber, where all radiation is assumed to be emitted vertically towards the glass rather than being scattered. For further development of the model, a less approximate method of calculating the Nusselt number would be advisable as well as including a temperature dependent air velocity through the dryer. A more extensive model for estimating the evaporation rate of the SAP-pouches would also improve the results, especially for larger numbers of SAP-pouches in the drying tower.

Table of contents

Nomenclature

A_{abs}	Collector absorber area (= glass area)	m²
A_{bag}	The effective area for evaporation of a SAP-pouch	m²
A_{bags}	Total effective evaporation area of SAP-pouches per shelf	m²
A_{eff}	Effective cross section area for the dryer airflow	m²
A_{inlet}	Collector inlet area	m²
A_{sides}	Collector side area	m²
a_w	Water activity	1
$C_{P, air}$	Specific heat capacity for air	J/(kg·K)
$C_{P, H2O}$	Specific heat capacity for steam	J/(kg·K)
D_H	Hydraulic diameter of the collector	m
E_{vap}	Total power required for evaporation for all SAP-pouches placed on a shelf in the dryer	W
G	Total solar irradiation	W/m²
G_e	Effective solar irradiation (heat absorbed by the absorber)	W/m²
$h_{con, in}$	Heat transfer coefficient for internal convection	W/(m²·K)
$h_{con, out}$	Heat transfer coefficient for external convection	W/(m²·K)
$h_{rad, in}$	Heat transfer coefficient for internal radiation	W/(m²·K)
$h_{rad, out}$	Heat transfer coefficient for external radiation	W/(m²·K)
m_b	Water mass flow	kg/s
m_{vap}	Water mass flow from SAP-pouch	kg/s
n	Number of bags per shelf in the dryer	1
Nu	Nusselt number for uniform surface heat flux	1
Pr_{air}	Prandtl number for air	1
P_w	Vapour pressure for water	Pa
P_{ws}	Water saturation pressure	Pa
R_{abs}	Absorber reflectance	1
Re_{air}	Reynolds number for air	1
R_{glass}	Glass reflectance	1
RH	Relative humidity	1
R_V	Specific gas constant for water vapour	J/(kg·K)
S	Number of shelves in the dryer	1
T_{abs}	Absorber temperature in the collector	K
T_{air}	Mean temperature of T_{in} and T_{out}	K
T_{amb}	Ambient temperature	K
t_{bottom}	Bottom insulation thickness	m
T_{glass}	Glass temperature in collector	K
T_{in}	Inlet temperature for a section	K
T_{out}	Outlet temperature for a section	K
t_{side}	Side insulation thickness	m
T_{sky}	Sky temperature	K
T_{wall}	Wall temperature of dryer	K
T_{wall}	Outer wall temperature in the collector	K
$T_{wall, in}$	Inner wall temperature in the dryer	K
$T_{wall, out}$	Outer wall temperature in the dryer	K
u_{air}	Collector inlet air velocity	m/s
u_{bags}	The air velocity surrounding the SAP-pouches	m/s

X	Air constant ($\varrho_{air} \cdot C_{P,\,air} \cdot u_{air} \cdot A_{inlet}$)	W/K
z	Additional heat gains for the outer walls of the dryer	W/m²
a_{abs}	Absorber absorbance	1
$\varDelta h_{vap,\,H2O}$	Enthalpy of vaporization for water	J/kg
ε_{abs}	Absorber emissivity	1
ε_{glass}	Glass emissivity	1
ε_{wall}	Collector outer wall emissivity	1
$\varepsilon_{wall,\,dryer}$	Dryer outer wall emissivity	1
λ_{air}	Air thermal conductivity	W/(m·K)
λ_{bottom}	Collector bottom insulation thermal conductivity	W/(m·K)
λ_{side}	Collector side insulation thermal conductivity	W/(m·K)
λ_{wall}	Dryer wall thermal conductivity	W/(m·K)
μ_{air}	Air dynamic viscosity	kg/(m·s)
ϱ_{air}	Air density	kg/m³
σ	Stefan-Boltzmann constant	W/(m²·K⁴)
τ_{glass}	Glass transmissivity	1

Acknowledgements

1 Introduction

The malnutrition in developing countries has proven to be a persistent problem over the decades and appears to remain unsolved despite the economic growth that has occurred in some of the countries. Among these developing countries is Mozambique, which had a Human Development Index (HDI) positioned at rank 180 out of 188 countries and territories in 2014 by the United Nations Developing Programme, despite the HDI value being 75 % higher than in 1980 (UNDP, 2015). Almost one-third of Mozambicans, most of them living in the south and centre regions, suffer from chronic food insecurity and the country is prone and sensitive to natural disasters such as drought and flooding (World Food Programme, 2016).

Even if a major number of Mozambicans are suffering from malnutrition, it is not due to insufficient harvests. The problem lies within the lack of technical solutions to preserve harvested food, where the current methods tend to lead to major losses and a poor product quality. Since Mozambique currently is lacking the economical means and infrastructure to support conventional preservation methods of non-developing countries, the food preservation technique should preferably be simple and independent of auxiliary energy sources and complex materials. An ongoing project at Lund University, suggests that solar thermal drying technology could be a part of the solution.

One method for preserving the fruit is using an indirect solar dryer consisting of a solar collector connected to a drying tower, which will be the main focus of this study. An indirect solar dryer uses a solar collector to heat air which is then transported to a drying unit which is protected from direct sunlight. Protecting the foods from direct exposure to sunlight, also known as indirect solar drying, could have some disadvantages which will be discussed further in this report. The drying tower holds bags filled with fruit juices for drying, which will be referred to as solar assisted pervaporation pouches, or SAP-pouches, which function as a more hygienic means of preserving fruit juices.

The aim of the study is to set up a mathematical model for an indirect solar thermal dryer that can be used to dry fruits in developing countries such as Mozambique. Furthermore, the model will be used to generate simulations to identify ways of improving the dryer performance. This will be done by setting up a base scenario in which a parameter analysis will be performed to find the most suitable dimensions and material properties. Once the parameters are identified they will be used to create a more optimal solar dryer. To perform the simulations, the model should be set up as a calculation tool which could also assist the project in Mozambique in the future.

2 Background

2.1 Solar thermal potential in Mozambique

As for many other sub-Saharan African countries, Mozambique is lacking sufficient access to modern energy. It has been estimated that about 587 million people in the Sub-Saharan region lack access to electricity and around 657 million people are relying on biofuels as the primary energy source. Although high quality energy is insufficient the primary energy sources of the region have a potential which has yet to be utilized, where the Sub-Saharan region has one of the highest levels of solar radiation worldwide (Piroschka Otte, 2014).

Although the economy of Mozambique is growing at a steady state and its government is making continuous efforts in electrifying the rural areas, the decentralized electrical grids of the country are known to be unreliable due to the costs and logistic problems of the diesel generators used for power production. Bearing this in mind, solar energy could be an important step towards a higher energy security as the large scale solar thermal potential is estimated to approximately 5 kWh/(m²·day), which could be used instead of electricity for various processes (Hammar, 2011). Solar thermal energy has higher potential regarding energy production and is a simpler technology than PV-panels, making it a better option for a developing country. The only downside is that thermal energy has a more limited use due to the produced heat having a lower energy quality than electricity. For this reason, solar thermal power is preferred to be used for heating purposes since no energy conversion is required. On the other hand, Mozambique is a tropical to sub-tropical country where the coolest parts of the year provide a 20 °C to 25 °C outdoor temperature in the southern lowland parts and around 15 °C to 20 °C outdoor temperature in the northern parts with higher altitude (McSweeney et al., 2012). Considering that the seasonal variations in temperature is just around 5 °C between the coldest months, being June, July and August and the warmest months being December, January and February, the energy demand for space heating could prove to be rather limited, especially in a modernized Mozambique with more well-insulated buildings (McSweeney et al., 2012).

A different field of use for solar thermal energy is fruit and crop drying, as food preservation could reduce the malnutrition significantly. Solar drying of harvested products is one of the most important potential applications of utilizing the incoming solar energy. In developing countries, conventional drying is the most commonly used methods e.g. open sun drying. But these methods come with some severe drawbacks in terms of quality, accuracy, capacity, economy, and handling, causing loss of the products during their drying which is estimated to be 30 % to 40 % of the total production in developing countries (Kumar et al., 2015).

2.2 Potential for solar thermal drying and SAP-pouches

Previous studies have found that Mozambique suffer 25 % to 40 % post-harvest losses of crops, mainly due to inadequate preservation methods and infrastructure (Phinney et al., 2015). During the harvest season, the fruit supply is considered to be nearly limitless. Due to the abundance of fruit, the local farmers find no need in planting fruit trees since the wild trees currently yield more fruit than they can sell or preserve during the rather short harvest season. The harvested fruit mainly consisting of mango, marula, tangerines, masala, mapfilwa, muquaqua and pineapple are placed on the ground on top of plastic weaves or residual stems from the harvest to dry in the sun. The supply of tools and kitchen utensils is limited, resulting in the major part of the food preparation being made by hand in pots placed directly on the ground. Having an inadequate drying method is a missed economic opportunity for Mozambique. Even if the fruits sold at the informal markets are near exclusively fresh, other processed products such as flour and paste are the most beneficial products to sell, as they can also be sold during drought and a low supply of fresh fruit. One of the problems with processing fruit is that it has proven to be too time consuming, resulting in negation of production of certain products. With a more effective and hygienic method of preserving the fruits Mozambique could seize greater economic opportunities as well as reduce the national malnutrition issue (Bratt & Ånger, 2015).

To find an applicable solution to the preservation issue, the end product quality must be considered as well as the resource demand for the process. Other preservation technologies such as canning or aseptic processing are economic on a large scale but will have a high energy demand, require access to clean water and a more developed infrastructure. The technology used for the drying process should preferably avoid these issues while maintaining an acceptable level of water activity a_w in the product. The water activity is defined as the ratio of the vapour pressure of the food and the saturation pressure of pure water at the same temperature according to equation (A).

$$a_w = \frac{P_W}{P_{WS}} \tag{A}$$

A lower water activity indicates that the product has less water available for chemical reactions and microbial growth. A water activity below 0,7 at ambient conditions prohibits any microbial growth of bacteria, yeast and mold thus insuring preservation of the product.

A technique currently under development is the solar assisted pervaporation (SAP). The so called SAP-pouches consist of textile coated with a membrane of polyurethane, see Figure 1, that allows water vapour to pass through the fabric while remaining impermeable to liquid water. These reusable
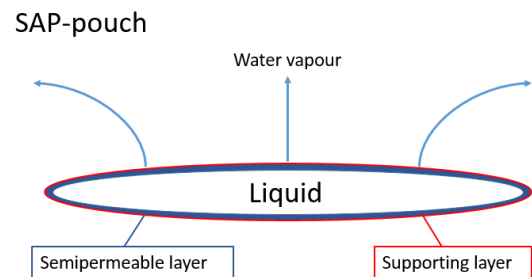

Figure 1   *Schematic figure of a solar assisted pervaporation (SAP) pouch.*

3

pouches can be filled with fruit juice or purée and then be dried either by direct or indirect solar heating while protecting the product from contamination. The SAP-fabric is hydrophilous, resulting in the fabric being in a saturated state during the entire drying process. Since the pouch will have a larger active evaporation area than an open vessel, the drying process will also be faster. The pouches should be placed horizontally, since a pouch placed vertically will cause the upper layer of the pouch dry out and thus reducing the effective evaporation area of the pouch. Studies by Phinney et. al prove that the SAP technology can provide a drying process of fruit juices and purées with water activities well below 0,7. One of the studied products was mango purée, which was dried from a water activity of 1,0 to 0,48 within 45 hours at a steady temperature of 40,5 °C. The drying time is strongly dependent on the ambient relative humidity, which in turn is dependent of the temperature, since a higher relative humidity will decrease the evaporation rate of the pouch. Another conclusion of the study was that an increased ambient wind velocity significantly decreases the drying time (Phinney et al., 2015). Pre-heating air in a solar collector would benefit from both of the conclusions that were made, since the temperature will increase which will lower the ambient relative humidity and could also be used to create a natural convective air flow through the collector (Augustus et al., 2002). In conclusion, SAP-technology combined with solar thermal collectors could provide with an effective and hygienic method of drying crops in developing countries. Having a natural convective air flow through the solar collector will be one of the design criterias for the simulated solar collector, since this will increase the drying speed while maintaining a construction independent of auxiliary energy sources.

2.3 Solar drying methods

To apply the solar drying as means of conserving the harvested fruit in Mozambique, several methods of constructing a solar dryer can be applied which generally can be divided into three different categories; direct-, indirect- and hybrid solar dryers which in turn can be either passive or active using auxiliary energy to improve the drying process. To evaluate the performance of a solar dryer, several parameters should be taken into account. The main performance parameters are the drying rate, the drying air temperature and relative humidity, the airflow rate, the end product quality and the economic costs and benefits (Augustus et al., 2002). The most important parameter to consider when designing the solar collector is the drying temperature, as this will partially determine the drying rate and the product quality in terms of health. According to the Orange Book by Tetra Pak (Tetra Pak, 1998), the drying temperature should be above 50 °C since bacteria will stop reproducing at this temperature. Furthermore, it would be possible to pasteurise fruit juices at any temperature exceeding 50 °C, but the pasteurisation time will decrease logarithmically with increasing temperature. As an example, increasing the temperature from 50 °C to 60 °C will decrease the drying time from 320 hours to 12 hours, which would be more reasonable for a solar dryer. However, Vitamin C will start degrading at temperatures above 50 °C meaning that too high drying temperatures could cause severe losses of nutrients. According to Randi Phinney, PhD student at the department of food technologies at Lund University, it is recommended to keep the drying temperature below 65 °C to preserve nutrients (Phinney et al., 2015).

4

2.3.1 Direct solar drying

A direct solar dryer is characterised by the product being directly exposed to solar irradiation, but there are several different variations of the method that can be applied. One method has been illustrated in Figure 2, where the foods are protected by a laye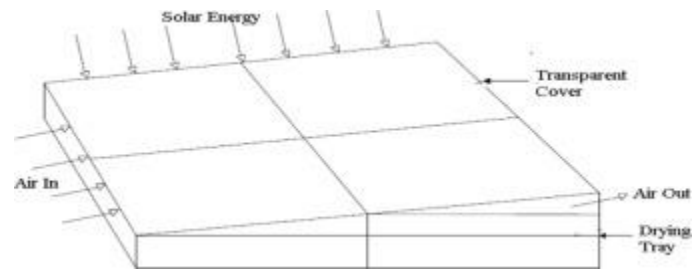r of glass. The simplest method is open direct solar drying, where the products are directly exposed to the ambiance. The main benefit of this method is that the material and maintenance costs can be kept to a minimum since any open surface will suffice for the drying process and no auxiliary power or fuels are required, reducing the economic costs to a minimum. The economic gains will, on the other hand, decrease compared with alternative methods of drying due to increased product losses from fungal growth, pests or unpredicted weather effects. In tropical countries such as Mozambique, the wet seasons of the year could have devastating effects on the products (Ekechukwua & Norton, 1997). The current method commonly used in developing countries is direct open sun drying, which suffers several drawbacks such as no control of the input parameters (e.g. temperature, wind velocity, humidity) and high degradation of the drying products (Kumar et al., 2015). The direct solar drying method will also expose the products to higher levels of UV radiation which will cause increased degradation of nutrients such as Vitamin C (Tikekar et al., 2011). The direct exposure to sunlight will also generate a higher surface temperature of the products which will cause further degradation of Vitamin C particularly during longer periods of time (Burdurlu et al., 2005).

Figure 2   Schematic figure of a direct solar dryer. Source: (Kumar et al., 2015)

A solution to the issues of the open dryer could be to add a transparent layer above the drying products. Direct closed solar dryers have a drying chamber which is an insulated box covered by a transparent cover made of glass or plastic and having air holes to allow air to enter and exit the chamber. The solar radiation penetrating the transparent layer will heat the products and the released water vapour from the products will be ventilated out of the box by either natural convection or a forced air flow using a fan. While the products become more protected against ambient conditions, the added transparent layer will cause optical losses as some solar irradiation will be reflected or absorbed by the transparent layer (Kumar et al., 2015).

5

2.3.2 Indirect solar drying

Indirect solar dryers utilize pre-heated air from a heat source to dry the products in a separate drying chamber (see Figure 3), preventing the products from being directly exposed to sunlight. The air flow throughout the dryer is generally forced using fans, but could also be generated by natural convection which would be a more preferable alternative for a developing country (Kumar et al., 2015). A major disadvantage that direct solar dryers have over indirect dryers is the direct exposure of the products to
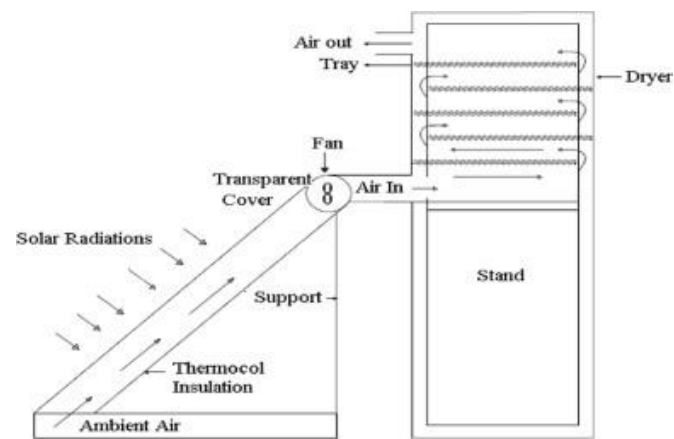

Figure 3   Schematic figure of an indirect solar dryer. Source: (Kumar et al., 2015)

sunlight. If the SAP pouches were to be heated by direct sunlight, the heat distribution of the bags content would be uneven. The upper parts of the bags would absorb the solar energy directly and thus heat up more quickly while the bottom parts would heat up at a slower rate. This could cause formation of a hardened layer of crust at the top of the bag (case hardening), preventing further evaporation and reducing the nutrient contents while the bottom layers of the bags would maintain a high moisture content (Mills-Gray, 1994).

The natural convective airflow through the dryer could be sufficient for the drying process since a higher air flow will cause less residence time of the air in the collector, meaning that the temperature will be lower and thus increase the drying time (Yaldýz & Ertekýn, 2001). Having a fan added to the dryer would on the other hand result in better control of the drying temperature, reducing the risk of destroying nutrients at high temperatures. The indirect forced convection dryers using fans have been reported superior in drying speed and product quality. Due to high drying rates and energy effectiveness, they have been observed suitable for low solar insolation and high humidity climate zones (Kumar et al., 2015). From an efficiency point of view, the increased air flow using a fan would decrease the temperature difference of the dryer and the ambience, resulting in reduced heat losses (Augustus et al., 2002). The increased airflow can be controlled to remain at an optimum, which has been observed to be 0,75 m³/s per square meter area (Tokar, 1997). However, this design could prove to be difficult to implement in Mozambique due to the low availability of electricity grids in the rural areas of the country (Hammar, 2011). It has also been observed that the efficiency of active solar dryers decreases at higher temperatures (Hossain et al., 2008).

The passive solar dryers have the benefit of being entirely independent of auxiliary energy sources while maintaining a good product quality. This design appears to be the most attractive option for rural areas, as the product quality is superior to the direct open drying method while still being economically competitive. The indirect solar drying method will in general decrease the drying time compared with open direct solar drying, meaning that the required drying area will be decreased (Ekechukwua & Norton, 1997).

2.3.3 Hybrid solar drying

A hybrid solar dryer combines the direct-
and indirect drying method, where a solar
collector is used to preheat air to a
transparent drying chamber where the
products can be directly exposed to
sunlight according to Figure 4. The hybrid
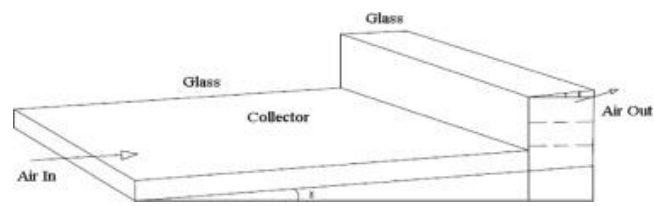dryers can be combined with auxiliary

Figure 4   *Schematic figure of a hybrid solar dryer.*
Source: (Kumar et al., 2015)

energy sources such as biomass for energy backup or PV-cells. One of the greatest benefits of
a hybrid solar dryer is that the drying rate is faster than any other current alternative while still
maintaining a good product quality (Kumar et al., 2015). On the other hand, more complex
constructions are likely to require a higher level of expertise to operate, making it a less
attractive alternative for the rural areas of Mozambique (Augustus et al., 2002). Constructing
the dryer for natural convection only (passive hybrid solar dryer) would be a more suitable
alternative, but would still maintain the risk of formation of case hardening in the SAP-
pouches inside the drying chamber.

3 Method and theory

3.1   Selecting the simulation program

The main goal of the study is to find theoretically suitable dimensions and material properties
for a solar collector which can be used to heat air to the right temperature for drying fruit. In
this study, a solar collector connected to a drying cabinet will be simulated in order to
estimate if the outlet temperature is sufficient for food preservation. To perform the
simulations, it is advisable to compute the calculations using a simulation program. A
simulation program will carry the benefit of flexibility, as any other user familiar with the
simulation program would be able to adjust the model to meet their demands. This is a
convenient property for the study at hand since the local designers in Mozambique would be
able to enter the desired dimensions and materials for the collector directly into the
simulation program. This does, however, require that the local designers have access to the
program and have been educated in using it properly.

For this model, Maple 2015 was selected as the simulation program due to the user friendly
and transparent calculation tools that are available. Maple 2015 is a math software which is
used to analyse, visualise and solve mathematical problems. The software will be used to
program a mathematical algorithm which can be used to represent a solar dryer by using
relevant equations. All equations used in the model can be found in Appendix A and it is
recommended to the reader of this report to print Appendix A on a separate paper, especially
when reading the results and discussion sections.

Another good candidate for the model would be Matlab, which could be used in combination
with different libraries e.g. Mollier charts or tables with steam and air properties. Another

7

qualified program is COMSOL Multiphysics, being a powerful simulation tool which utilizes built-in physical models to solve the user defined problems and would be likely to generate a rather accurate 3-D simulation of the model, but is on the other hand lacking the transparency of the calculations which both Maple and Matlab would have. But bearing in mind that model should be kept simple, Maple is for all intents and purposes a sufficient tool for building a good model.

3.2 Modelling the dryer in Maple 2015

For this study, an indirect solar dryer will be modelled by setting up and solving relevant equations in Maple 2015. The model will be split into two parts; a collector and a dryer, see Figure 5 for orientation, since the equations for these two parts will differ. The output air temperature of the collector will then be used as an input temperature for the dryer. The collector will have an energy source, the solar irradiation G passing through a single glass layer, while the dryer will only consist of different thermal losses. An additional heat gain will be added to the dryer to simulate the effects of solar irradiation of the dryer, but this will not be included in the base scenario. The dryer will on the other hand, unlike the collector, have an internal mass flux of water vapour from the SAP-pouches. The cross section areas for both parts are rectangular, but can have different dimensions. Both the collector and the dryer are insulated on the sides and have an air flow passing through them according to Figure 5 and all external walls are exposed to the ambiance.

Since maintenance of the dryer is required to be kept to a minimum, the design should not include any form of electronics or complex materials. For this reason, the air flow should only occur due to natural convection of the dryer where the temperature rise is the driving force. However, to simplify the problem the volumetric air flow is assumed to be known and constant. For a complete summary of the assumptions, see section 3.3 below. The model will be set up for a base scenario according to results section followed by a parameter analysis of the base scenario.
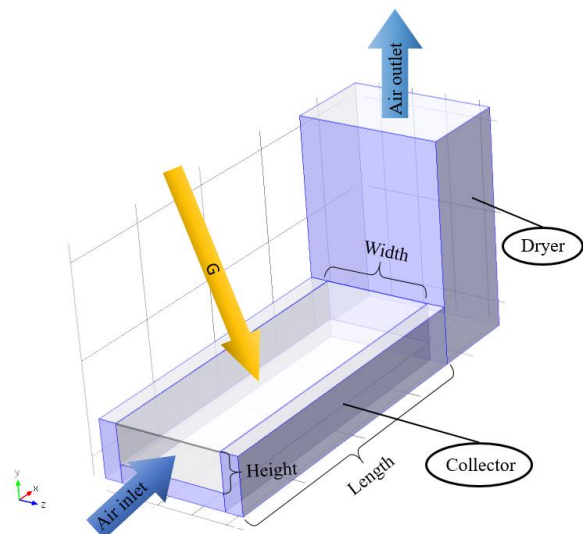

Figure 5   *Schematic figure of the model. The solar dryer is consisting of two parts: the collector and the dryer. The collector consists of a glass layer on the top, insulation on the sides and the bottom and an absorber plate on top of the bottom insulation layer. The dryer is insulated on the sides and contains shelves with SAP-pouches.*

3.3   Assumptions

- The collector and dryer are in steady state for a constant solar irradiation. In reality the solar radiation will vary with time and weather conditions.
- No air leakages.
- The collector inner sides are assumed to have the mean temperature of the absorber and the glazing of the collector.
- The temperatures of the SAP-pouches are equal to the surrounding air temperature and the bags are not dried out. In practise the evaporation rate from the SAP-pouches will differ when the dryer is warming up since the pouch temperature will increase, absorbing heat.
- The parameters ρ, C_P, μ, λ_{air} and Pr have been assumed to be constant for 300 K and 1 atm.
- The inner sides of the collector will not reflect any radiation. Instead, all heat radiation is reflected between the absorber and the glass. Furthermore, the heat radiation from the absorber to the glass is also assumed to be normal to the absorber. In practise the heat will radiate in several directions from the absorber and the glass.
- Fully developed laminar air flow for Re < 3000 and fully developed turbulent air flow for $3000 \leq Re \leq 5 \cdot 10^5$. For the turbulent interval, the characteristic length of the collector/dryer must be at least 10 times greater than the hydraulic diameter.
- No heat transfer between SAP-pouches.
- The ambient temperature is within the interval 0 °C < T_{amb} < 100 °C, the valid interval for using Antoine's equation for saturation pressure.
- The glass does not absorb any sunlight ($a_{glass} = 0$).
- The collector sides and bottom and the dryer walls do not absorb any sunlight on the outside. Additional heat gains of the dryer will be added independently of the solar irradiation G.
- The convective heat transfer coefficient $h_{con, out}$ is assumed to be a constant value of 20 W/(m²·K) (Sekhar et al., 2009) (Kumar Moningi, 2016).
- The outward heat radiation of the side areas of the collector and the dryer walls are assumed to radiate 50 % towards the sky (T_{sky}) and 50 % towards the ground (T_{amb}).

3.4   The collector

To simulate the collector, four variable temperatures T_{glass}, T_{air}, T_{abs} and T_{wall} have been included in the model representing the mean temperatures for the glass, air, absorber and external walls respectively for a section of the collector. These four temperatures will act as four variables which will require four equations to be solved, which will be done by setting up energy balances. The sections mentioned are small sections of the collector length, where the outflow temperature of the air in one section will be the inflow temperature of the air in the following section. As an example, if the collector is 1 m long and divided into 10 sections, the four mean temperatures listed above will be calculated for the first section located between 0

9

cm to 10 cm from the inlet of the collector. The outlet air temperature of the first section will then be used as inlet air temperature of the second section located between 10 cm to 20 cm from the collector inlet. Figure 6 illustrates the various energy flows that will occur for a section of the collector and affect the temperatures. This process is repeated for the full collector length in order to obtain the temperature of the outlet of the collector, which will serve as the inlet air temperature of the dryer. The reason for dividing the collector into several sections will be explained below.
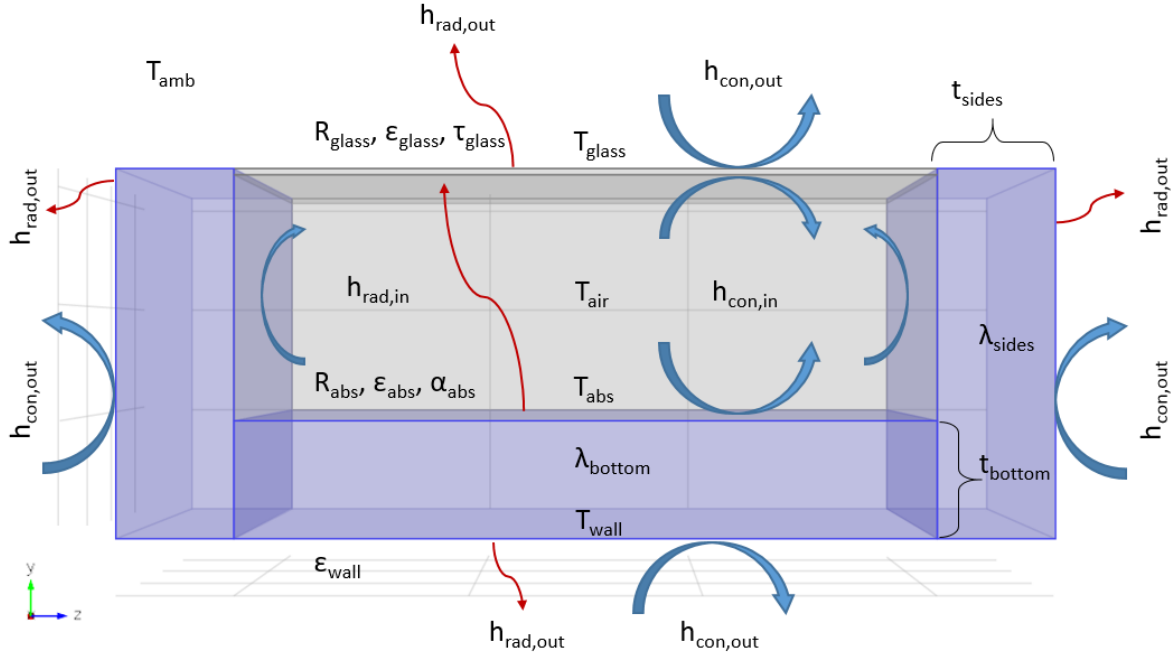

Figure 6   Schematic figure for all energy flows and temperatures that are included in the model for the collector. Energy balances for the glass, air flow, absorber and outer wall of the collector will be set up according to this figure. Blue arrows are representing convective heat transfer and red arrows are representing radiative heat transfer. For further explanation of the parameters, see the Nomenclature section.

To be able to set up the four energy balances required to calculate T_{glass}, T_{air}, T_{abs} and T_{wall}, one must first understand the various energy flows of the collector. Looking back at Figure 5, the solar irradiation G will irradiate the glass layer of the collector. A portion of this radiation will be able to pass through the glass depending on the glass transmissivity τ_{glass} and hit the absorber. Depending on the absorbance of the collector a_{abs} and how much solar radiation that is being reflected between the absorber and the glass, R_{abs} and R_{glass}, the absorber will be able to absorb a certain amount of energy. The energy absorbed by the absorber will result in a temperature rise of the absorber plate.

The absorber temperature will depend on the magnitude of various energy losses. The energy losses are limited to the three ways heat can be transferred; by radiation, convection or conduction. The red arrows of Figure 6 are representing heat being transferred from one surface to another through radiation. The external radiative heat transfer of the collector illustrated in Figure 6 are either radiating towards the ground or the sky. Since the air within the collector is a fluid and the height of the collector is very short, the air will not be able to absorb any heat radiation. The radiative heat transfer of the collector is the only reason dividing the collector into sections is necessary. As shown in equation (3) and (4) below, the

10

radiative heat transfer coefficient is dependent on the temperature between two surfaces to the power of four. Since the air temperature of the collector will be warmer near the outlet than it will be near the inlet, the radiative heat transfer coefficient will vary throughout the collector. This means that dividing the collector into as small sections as possible and calculating the radiative heat transfer coefficient for each individual section is the best method for taking the variations into consideration. The radiative heat transfer will also vary depending on the emissivity ε, which represents how much heat that is emitted from a surface. A low-emittance absorber is better for generating high absorber temperatures, since less heat will be emitted away from the surface of the absorber.

The blue arrows of Figure 6 are representing the convective heat transfer of the collector. Convective heat transfer will occur both on the inside and the outside of the collector, but since the outside of the collector can be affected by wind the convective heat transfer coefficient on the outside of the collector is likely to be higher. The internal convective heat transfer will affect all internal walls for the collector; the absorber, the sides and the glass. The convective heat transfer from the absorber to the air will represent the heat that is being transferred to the air. On the other hand, convective heat transfer between the collector sides and glass will absorb heat from the air if these are colder than the air.

The final energy flows to be described in Figure 6 is the conductive heat transfer. The conductive heat transfer represents heat that is being transferred through a solid material, which in the case of the collector is the side and bottom insulation. When the absorber temperature rises, heat will be transferred from the absorber to the outside of the bottom of the collector. Depending on the thermal conductivity of the insulation of the bottom and sides, λ_{bottom} and λ_{sides} respectively, as well as the thicknesses of the insulation layers, more or less heat will be transferred from the inner walls of the collector to the outer walls. In this model the outer walls of the sides and bottom of the collector have been regarded as a single unit which has the same temperature on the sides and the bottom.

Now that the different energy flows have been identified in terms of heat transfer, four energy balances for four boundaries will be set up for the collector according to Figure 6 to solve the four variable temperatures; the glazing, the air flow inside the collector, the absorber and the external walls.

3.4.1 Calculating the effective solar irradiation G_e

To calculate the effective solar irradiation heating up the absorber, the optical parameters of the glazing and the absorber must be taken into account. The glazing will let through solar radiation to the absorber depending on the transmissivity τ_{glass} of the glass and the absorber will absorb the radiation according to the absorbance a_{abs} of the absorber. The radiation will also be reflected between the glazing and the absorber depending on R_{abs} and R_{glass}. The resulting equation for G_e can be found in equation (1).

$$G_e = \frac{G \cdot \tau_{glass} \cdot \alpha_{abs}}{1 - R_{abs} \cdot R_{glass}} \tag{1}$$

3.4.2 Setting up the equation for the glazing

The equation set up for the glazing will be done according to the boundary energy balance illustrated in Figure 6, resulting in equation (2). As seen in Figure 6, there are two energy flows entering the glass; convection from the air flow and radiation from the absorber. The amount of energy transferred to the glass will depend on the heat transfer coefficients, the affected glass area and the temperature differences. The first term and second terms of equation (2) corresponds to the ingoing convective and radiative heat transfer to the glass respectively. The two remaining terms are negative and are corresponding to the convective heat losses from the glass to the ambient air and the radiative heat losses from the glass to the sky temperature. Since all ingoing energy flows to the glass must be equal to all outgoing energy flows, an energy balance can be set up according to equation (2), resulting in the first equation of the model.

$$h_{con,in} \cdot A_{abs} \cdot \left(\frac{T_{in} + T_{out}}{2} - T_{glass}\right) + h_{rad,in} \cdot A_{abs} \cdot (T_{abs} - T_{glass}) - h_{con,out} \qquad (2)$$
$$\cdot A_{abs} \cdot (T_{glass} - T_{amb}) - h_{rad,out} \cdot A_{abs} \cdot (T_{glass} - T_{sky}) = 0$$

While $h_{con,\,out}$ is assumed to be constant, expressions must be found for the remaining heat transfer coefficients. The heat transfer coefficients for radiation can be calculated according to equation (3) for $h_{rad,\,in}$ and according to equation (4) for $h_{rad,\,out}$ (Incropera & Dewitt, 2002). The heat radiation from the absorber is emitted against the glass temperature and the heat radiation from the glazing is emitted against the sky temperature.

$$h_{rad,in} = \frac{\dfrac{1}{\dfrac{1}{\varepsilon_{abs}} + \dfrac{1}{\varepsilon_{glass}} - 1} \cdot \sigma \cdot \left(T_{abs}^4 - T_{glass}^4\right)}{T_{abs} - T_{glass}} \qquad (3)$$

$$h_{rad,out} = \frac{\varepsilon_{glass} \cdot \sigma \cdot \left(T_{glass}^4 - T_{sky}^4\right)}{T_{glass} - T_{sky}} \qquad (4)$$

To calculate the internal convective heat transfer coefficient $h_{con,\,in}$ the definition of the Nusselt number can be used provided that air flow characteristics are known. In this case the collector should not be connected to a fan, resulting in the air flow being driven solely through natural convection. However, to simplify the problem the air flow is assumed to be forced for a fix air velocity. For low values of the Reynold number (<3000) the flow is assumed to be a fully developed laminar flow. This means that the Nusselt number will only vary depending on the cross section characteristics, resulting in the Nusselt number becoming a constant value for the entire collector length, see Appendix B. The main reason for using this method is because the cross section is non-circular which will cause a different air velocity profile over the cross section since the flow velocity will be decreased in the corners due to surface friction, resulting in the correlations used for circular pipes being less accurate (Incropera & Dewitt, 2002).

For higher values of the Reynold number ($3000 \leq Re \leq 5 \cdot 10^5$) the air flow is regarded as a fully developed turbulent flow. In this interval Gnielinski's correlation can be used to obtain the Nusselt number, which is shown in equation (5) where the friction factor *f* is defined according to equation (6) (Incropera & Dewitt, 2002).

$$Nu = \frac{\left(\frac{f}{8}\right) \cdot (Re_{air} - 1000) \cdot Pr_{air}}{1 + 12{,}7 \cdot \left(\frac{f}{8}\right)^{\frac{1}{2}} \cdot (Pr_{air}^{\frac{2}{3}} - 1)} \tag{5}$$

$$f = (0{,}790 \cdot \ln(Re_{air}) - 1{,}64)^{-2} \tag{6}$$

When the Nusselt number has been, $h_{con,\,in}$ can be calculated using the definition of the Nusselt number according to equation (7) (Incropera & Dewitt, 2002). Note that the Nusselt number will be valid for all inner sides of the collector and that the same method is used to calculate the convective heat transfer coefficient for the dryer.

$$Nu = \frac{h_{con,in} \cdot D_h}{\lambda_{air}} \tag{7}$$

The hydraulic diameter of the rectangular cross section area is defined according to equation (8) (Incropera & Dewitt, 2002).

$$D_h = \frac{2 \cdot Height \cdot Width}{Height + Width} \tag{8}$$

3.4.3 Setting up the equation for the air flow

For the air flow energy balance, the mass balances of the air and the water vapor needs to be considered as well as the convective heat transfer within the collector. In this model, the water molecules of the air flow and the pure air flow are treated separately in order to make better calculations for the relative humidity. This will become more relevant within the dryer. An alternative way of taking the water content of the air into consideration would be to use an averaged density and heat capacity for the two medias.

The absorber will transfer heat through convection from the absorber to the air mass while heat losses are occurring through convective heat transfer towards the glazing, which has been included in the energy balance for the air flow, equation (9). The first term of equation (9) stands for the convective heat transfer between the absorber and the air flow, where the average air temperature for a section is used. The second term corresponds to the convective heat transfer between the inner wall of the collector and the air flow, where the inner wall is assumed to have the average temperature of the absorber and the glass temperature. Convective heat losses from the air will reduce the air temperature and has been taken into account in the model as the third term of equation (9).

The fourth and fifth term of equation (9) correspond to how much energy that is absorbed by the air flow, which also contains some water molecules, resulting in the air mass and the

13

water vapor being heated up. Since ρ_{air}, $C_{P, air}$, u_{air} and A_{inlet} are all considered to be constants in the model, the constant X is defined according to equation (10), which will determine how much energy that is required to heat up the air 1 °C. Now that all five terms of equation (9) have been identified, expressions for some of the parameters of the equation will be required, starting with m_h.

$$h_{con,in} \cdot A_{abs} \cdot \left(T_{abs} - \frac{T_{in}+T_{out}}{2}\right) + h_{con,in} \cdot A_{sides} \cdot \left(\frac{T_{abs}+T_{glass}}{2} - \frac{T_{in}+T_{out}}{2}\right) - \qquad (9)$$
$$h_{con,in} \cdot A_{abs} \cdot \left(\frac{T_{in}+T_{out}}{2} - T_{glass}\right) - (T_{out} - T_{in}) \cdot X - (T_{out} - T_{in}) \cdot C_{P,H2O} \cdot$$
$$m_h = 0$$

$$X = \rho_{air} \cdot C_{P,air} \cdot u_{air} \cdot A_{inlet} \qquad (10)$$

The mass flow of the water vapor m_h will be constant throughout the entire collector since no additional mass fluxes of water are present. Due to this fact, the absolute humidity for the collector can be calculated from the relative humidity of the inlet air. To calculate the absolute humidity, the saturation pressure for water needs to be calculated for the ambient temperature using Antoine's equation, equation (11), where P_{ws} is the saturation pressure of water at the temperature T and A, B and C are constants which are selected for the temperature. Once the saturation pressure for water has been found, the definition of relative humidity can be used to find the partial pressure of the water vapor in the air, see equation (12). The mass flow of water can then be calculated using equation (13), which is derived from the ideal gas law (Department of Chemical Engineering of Lund University, 2013).

$$\log(P_{ws}) = A - \frac{B}{T + C} \qquad (11)$$

$$RH = 100 \cdot \frac{P_w}{P_{ws}} \qquad (12)$$

$$m_h = \frac{P_w}{R_V \cdot T_{amb}} \cdot A_{inlet} \cdot u_{air} \qquad (13)$$

3.4.4 Setting up the equation for the absorber

According to Figure 6, the absorber plate will have heat losses through convection and radiation on the top side while the insulation layer will result in a conductive heat transfer on the bottom side (see equation (14)). The effective solar radiation G_e will act as a heat source for the plate. The calculations for the radiation towards the glass can be found in equation (15). In order to take the collector sides into account in the model, the conductive heat losses of the sides have been included in the absorber equation. Note that the heat losses from the collector sides are included in the equation for the absorber, where the inner wall temperature of the collector is assumed to have the mean temperature of the absorber temperature and

14

the temperature of the glazing. This simplification has been made since the heat transfer from the collector sides will be minor in comparison to the absorber plate due to the lower temperature and smaller area, but it is possible to include more equations in the model where the inner collector wall temperature is also calculated. Also note that equation (14) has been divided by A_{abs}, which will also be done for the following energy balance equations for the collector.

$$G - h_{con,in} \cdot \left(T_{abs} - \frac{T_{in}+T_{out}}{2}\right) - h_{rad,in} \cdot \left(T_{abs} - T_{glass}\right) - \frac{\lambda_{bottom}}{t_{bottom}} \cdot \tag{14}$$
$$\left(T_{abs} - T_{wall}\right) - \frac{\lambda_{side}}{t_{side}} \cdot \frac{A_{sides}}{A_{abs}} \cdot \left(\frac{T_{abs}+T_{glass}}{2} - T_{wall}\right) - h_{con,in} \cdot \frac{A_{sides}}{A_{abs}} \cdot$$
$$\left(\frac{T_{abs}+T_{glass}}{2} - \frac{T_{in}+T_{out}}{2}\right) = 0$$

$$h_{rad,in} = \frac{1}{\frac{1}{\varepsilon_{abs}} + \frac{1}{\varepsilon_{glass}} - 1} \cdot \sigma \cdot \frac{T_{abs}^4 - T_{glass}^4}{T_{abs} - T_{glass}} \tag{15}$$

3.4.5 Setting up the equation for the outer walls of the collector

In order to set up a more simple expression for the energy balances of the outer walls of the collector, the outer bottom area of the collector is assumed to have the same temperature as the outer side walls of the collector. A more extensive model would include two different temperatures for the outer sides and bottom, but the simplification will suffice to generate approximate temperatures. After all, it is the air temperature that is the most important temperature.

As shown in Figure (6), heat will be transferred from the inside of the collector through the side and bottom layer of insulation, which will heat up the outer unglazed edges of the collector. Heat will be conducted through the insulation on the bottom of the collector, which represents the first term of equation (16), as well as through the insulation on the sides of the collector which represents the second term of the equation. Both terms are positive, meaning that they are energy inflows to the outer walls.

$$\frac{\lambda_{bottom}}{t_{bottom}} \cdot \left(T_{abs} - T_{wall}\right) + \frac{\lambda_{side}}{t_{side}} \cdot \frac{A_{sides}}{A_{abs}} \cdot \left(\frac{T_{abs}+T_{glass}}{2} - T_{wall}\right) - h_{con,out} \cdot \tag{16}$$
$$\frac{(A_{abs}+A_{sides})}{A_{abs}} \cdot \left(T_{wall} - T_{amb}\right) - h_{rad,out1} \cdot \left(T_{wall} - T_{amb}\right) - h_{rad,out1} \cdot$$
$$\frac{A_{sides}}{2 \cdot A_{abs}} \cdot \left(T_{wall} - T_{amb}\right) - h_{rad,out2} \cdot \frac{A_{sides}}{2 \cdot A_{abs}} \cdot \left(T_{wall} - T_{sky}\right) = 0$$

The remaining terms of equation (16) are negative, meaning that they represent the energy losses of the outer walls. The energy losses will occur by convection and radiation on the sides and bottom respectively according to Figure (6). The convective heat losses on the outside of the collector is assumed to be uniform for both the sides and the bottom, resulting in the third term of the equation, but the radiation will differ. For the bottom side of the collector, the heat will radiate from the wall to the ground, which has the same temperature as T_{amb}, but the sides will partially radiate towards the sky. For this reason, half of the radiation losses of the outer sides of the collector is assumed to radiate towards T_{amb} while the other

15

half will radiate towards T_{sky}. The expressions for the radiative heat transfer coefficients are calculated using the same method as for the glazing, resulting in equation (17) or (18) depending on which temperature the outer walls are radiating towards.

$$h_{rad,out1} = \varepsilon_{wall} \cdot \sigma \cdot \frac{T_{wall}^4 - T_{amb}^4}{T_{wall} - T_{amb}} \tag{17}$$

$$h_{rad,out2} = \varepsilon_{wall} \cdot \sigma \cdot \frac{T_{wall}^4 - T_{sky}^4}{T_{wall} - T_{sky}} \tag{18}$$

Now that the equations (2), (9), (14) and (16) have been defined and expressed as functions of T_{abs}, T_{glass}, T_{out} and T_{wall}, the equation system can be solved for all temperatures. In the built calculation tool the equation system is solved for a user defined amount of times (resolution). The idea of splitting the collector section into smaller sections and solving the equations for these sections is to create a more accurate result, since the radiative heat transfer coefficients will vary with the collector length.

3.5   The dryer

The calculations for the dryer has been made in a similar manner as for the collector, while also taking the mass flux of the water evaporating from the SAP-pouches into account. A schematic picture of a section of the dryer for which the equations are solved can be found in Figure 7, where the SAP-pouch is placed in the center. Unlike the collector, the resolution is defined by the number of shelves S that the dryer has. The equation system will consist of three equations; one for the inner walls, one for the outer walls and one for the air flow.
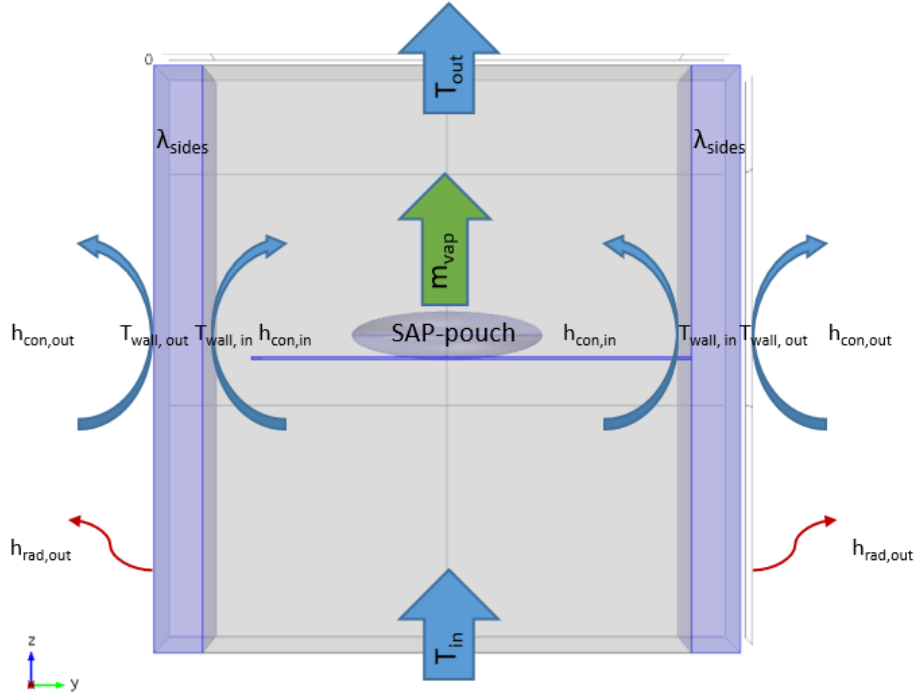

Figure 7   Schematic figure for all energy flows and temperatures that are included in the model for the dryer. Energy balances for the air flow, inner and outer wall of the collector will be set up according to this figure.

3.5.1 Setting up the equation for the inner walls of the dryer

Using the same method as for the collector, the equation for the energy balance of the inner wall can be written according to equation (19), where the walls will absorb heat from the air flow through convection and loose heat through the insulation layer of the dryer. Note that the radiation has been neglected. The reason why the radiation can be neglected is because the radiation is assumed to only be emitted perpendicularly from a surface. This means that there will be no radiative heat transfer between the inner walls, since the temperature difference between one side of the wall and the opposite side will always be equal.

$$h_{con,in} \cdot \left(\frac{T_{in} + T_{out}}{2} - T_{wall,in} \right) - \frac{\lambda_{dryer}}{t_{side}} \cdot \left(T_{wall,in} - T_{wall,out} \right) = 0 \qquad (19)$$

17

The convective heat transfer coefficient $h_{con,\,in}$ is calculated in the same manner as it was for the collector, see equation (7)-(8), where the Reynold number of the dryer will determine the value.

3.5.2 Setting up the equation for the outer walls of the dryer

The energy balance for the outward sides of the dryer was set up according to the same method used for the collector sides in section 3.5.5, meaning that half of the heat radiation will radiate towards the ground and half will radiate towards the sky. The resulting equation can be found in equation (20). One parameter that has been added to the energy balance for the outer walls of the dryer is the additional heat gains z. The additional heat gains represent the average solar irradiation of all four outer walls of the dryer. The additional heat gains will increase the outer wall temperature of the dryer, which will reduce the heat losses through the walls or, if the outer walls are warmer than the inner walls, add more heat to the air. For the base scenario the additional heat gains have been set to 0 W/m², but the effects of adding heat gains will also be studied.

$$\frac{\lambda_{dryer}}{t_{side}} \cdot \left(T_{wall,in} - T_{wall,out}\right) - h_{con,out} \cdot \left(T_{wall,out} - T_{amb}\right) - \frac{1}{2} \cdot \qquad (20)$$
$$h_{rad,out1} \cdot \left(T_{wall,out} - T_{amb}\right) - \frac{1}{2} \cdot h_{rad,out2} \cdot \left(T_{wall,out} - T_{sky}\right) + z = 0$$

The expressions for $h_{rad,\,out1}$ and $h_{rad,\,out2}$ are set up according to equation (17) and (18), where ε_{wall} now is the value of the emissivity of the dryer walls.

3.5.3 Setting up the equation for the dryer air flow

For the dryer air flow, the same method used in section 3.4.3 for the collector air flow is used with the addition of a mass flux of water vapor from the SAP-pouches. This means that the calculations need to include an accumulation of the water molecules from shelf to shelf. For the first shelf, the inlet mass flux of water will be according to the absolute humidity in the collector while the outlet mass flux will also have gained water from the SAP-pouches of the first shelf. The outlet mass flux of water from the first shelf will then be used as input for the inlet mass flux of water for the second shelf. Also note that the shelf is placed in the center of the dryer section, meaning that the SAP-pouch will have the section mean air temperature at steady state. The full expression used for the dryer air flow can be found in equation (21).

$$\left(T_{in} - T_{out}\right) \cdot X - h_{con,in} \cdot A_{sides} \cdot \left(\frac{T_{in}+T_{out}}{2} - T_{wall,in}\right) + \left(T_{in} - T_{out}\right) \cdot \qquad (21)$$
$$Cp_{H2O} \cdot m_h + \left(\frac{T_{in}+T_{out}}{2} - T_{out}\right) \cdot Cp_{H2O} \cdot m_{vap} - E_{vap} = 0$$

The water mass flow from the SAP-pouches will absorb heat in two steps. First, the water will need to evaporate from the pouches, where the enthalpy of vaporization for water will determine how much energy that will be absorbed. This energy will be referred to as E_{vap} and is defined according to equation (22).

18

$$E_{vap} = m_{vap} \cdot \Delta h_{vap,H2O} \tag{22}$$

Secondly, the evaporated water will be cooled off while being transported from the center of the dryer section to the section outlet (see term 4 of equation (21)). The inlet water mass flux m_b will on the other hand be cooled from the inlet temperature of the section to the outlet temperature of the section, according to term 3 of equation (21).

Finally, and expression for the mass flux from the SAP-pouches m_{vap} must be found. This mass flux will affect the dryer outlet temperature as well as the absolute humidity of the dryer. A lower dryer temperature and a higher absolute humidity would result in a higher relative humidity, which would increase the resistance of the evaporation rate and thus result in a longer drying time. Having mentioned this, the expression for m_{vap} is the most important factor for determining the drying time but also the most complicated expression to formulate. The mass flux will depend on the difference in partial pressure of water on the inside and on the outside of the pouches as well as the material that is being used. In addition to this, the drying rate will differ depending on if the pouch is still being heated up, at steady state or if the pouch has been dried out (Phinney et al., 2015). To solve this problem, the results from an empirical study of drying rates have been used to find an approximate expression for m_{vap}. The values from the study were obtained after measuring the evaporation rate of SAP-pouches within the relative humidity range of 4,7 % to 10,4 %, the air velocity range of 0,9 m/s to 4 m/s and a temperature range from 39,2 °C to 56,8 °C. A total of 24 measurements were made. To form an accurate equation based on the measurements the equation should include the relative humidity, the air velocity as well as the temperature, but since the expression used for the relative humidity is already based on the temperature (see equation (13)) the decision was made to only use the relative humidity and the air velocity as parameters. The values used for finding an expression for m_{vap} have been plotted as a function of the relative humidity for different air velocities in Figure 8 and the expression used for calculating m_{vap} in the model can be found in equation (23).
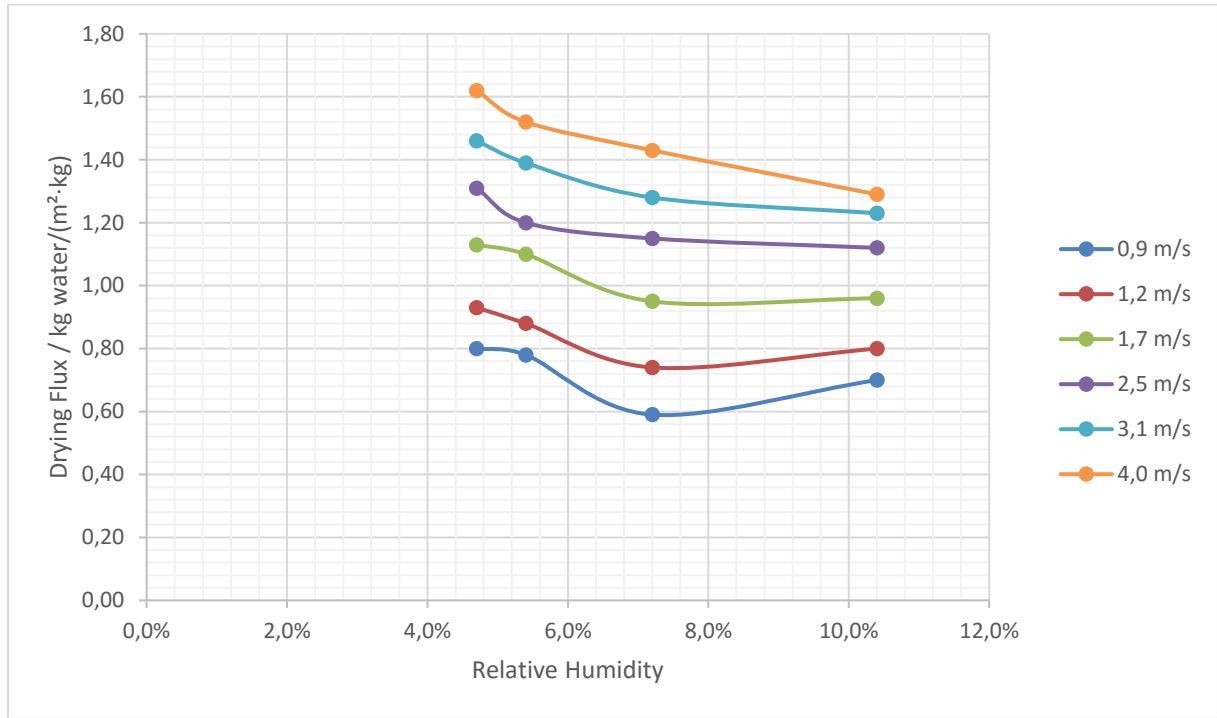
19

Figure 8   *Experimental values for the drying rate of SAP-pouches for different air flow velocities and relative humidity.*
Source: Phinney, R. Unpublished data. Department of Food Technology, Engineering and Nutrition. Lund University

$$m_{vap} = \frac{A_{bags}}{3600} \cdot \left(-1{,}0015 \cdot u_{bags} - 0{,}9565 \right) \cdot RH + 0{,}3088 \cdot u_{bags} + 0{,}6297 \qquad (23)$$

Note that the velocity used in equation (23) is not the inlet air velocity of the solar collector. The air velocity will naturally change when entering the dryer depending on the inlet area of the dryer, where a smaller cross section would increase the velocity which according to Figure 8 would benefit the evaporation rate. In addition to this, the SAP-pouches will also obstruct the air flow through the collector, see Figure 9, reducing the effective cross section area of the air flow even further. This effect will become more significant if more bags are placed on each shelf or if the shelves are designed to partially block the air flow. A potential problem could be if the size of the SAP-pouches would decrease during the drying time when water is being removed, resulting in a lower air flow velocity surrounding the bags. This is however not something that has been included in the model.
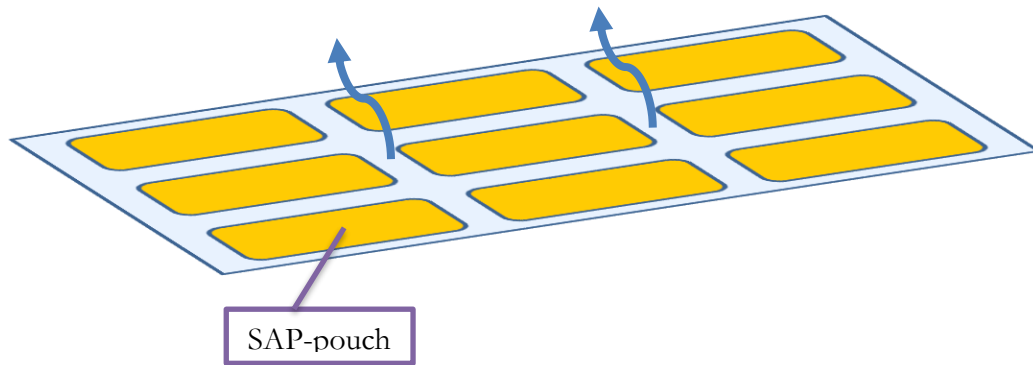
Figure 9   *Illustration of the increased air flow velocity surrounding the edges of the SAP-pouches.*

4 Results

4.1 The base scenario

Previous research for solar collector performances have been made at the University of Lund as a part of a master thesis work[1], where one of the studies included construction and testing of a solar dryer. The built solar dryer had a very typical appearance for a solar dryer, being similar to the dryer displayed on the cover page of this report. The solar dryer was built mainly out of plywood boards with an additional centimetre of styrofoam attached to the bottom of the collector for additional insulation. A very important thing to keep in mind is that the measurements of the dryer were only performed indoors, which would result in reduced convective losses as well as reduced radiative losses. The fact that the tests were carried out in Sweden will also grant this solar dryer different ambient conditions compared with Mozambique, since the ambient temperature, relative humidity and solar irradiation are likely to be lower in a Nordic country. However, since the built solar dryer had a very conventional design it's still relevant to use this design as the base scenario for this report.

The dimensions used for the base scenario can be found in Table 1. The air flow of the dryer is assumed to flow solely in the y-direction, see Figure 5, meaning that there is not any bottom or top side insulations of the dryer since these are the out- and inlets of the dryer. The collector parameters used can be found in Table 2 and the dryer parameters used can be found in Table 3. For parameter explanation see the Nomenclature section. The parameters selected for air and water vapour can be found in Table 4 and have been selected for a

---

[1] Andersson, L. Unpublished data. Department of Energy and Building Design. Lund University

temperature of 300 K. The ambient relative humidity is set to 37 %. The external heat transfer coefficient is set to 20 W/(m²·K), which can be considered to be a reasonable value for outdoor conditions (Sekhar et al., 2009) (Kumar Moningi, 2016).

Table 1   The selected dimensions for the modelled collector and dryer of the base scenario.

	Collector	**Dryer**	**Unit**
Height	0,22	0,6	m
Length	1,7	0,4	m
Width	0,6	0,6	m
t_{side}	0,01	0,01	m
t_{bottom}	0,02	-	m

Table 2   The selected parameters used for the modelled collector of the base scenario.

Collector parameter		**Unit**
G	700	W/m²
R_{abs}	0,1	1
R_{glass}	0,1	1
u_{air}	0,2	m/s
α_{abs}	0,9	1
ε_{abs}	0,9	1
ε_{glass}	0,837	1
ε_{wall}	0,95	1
λ_{bottom}	0,049	W/(m·K)
λ_{side}	0,13	W/(m·K)
τ_{glass}	0,9	1

Table 3   The selected parameters used for the modelled dryer of the base scenario.

Dryer parameter		**Unit**
A_{bag}	0,018	m²
n	10	1
S	6	1
$\varepsilon_{wall, dryer}$	0,9	1
λ_{wall}	0,13	1

Table 4 *The selected parameters used for the air and water vapor in the model. Note that all values are considered to be constant.*

Parameter		Unit
$C_{P, air}$	1007*	J/(kg·K)
$C_{P, H2O}$	1859**	J/(kg·K)
Pr_{air}	0,707*	1
R_V	461**	J/kg·K
T_{amb}	298,15	K
T_{sky}	278,15	K
u_{air}	0,2	m/s
$\Delta h_{vap, H2O}$	$2,26 \cdot 10^6$**	J/kg
λ_{air}	0,0263*	W/(m·K)
μ_{air}	$1,841 \cdot 10^{-5}$*	kg/(m·s)
ϱ_{air}	1,1614*	kg/m³

(Incropera & Dewitt, 2002)
** (Department of Chemical Engineering of Lund University, 2013)

The results for the base scenario for the collector air temperatures can be found in Figure 10. Five different simulations have been performed for different air velocities since the air flow will vary in a solar dryer driven only by natural convection. The interval has been selected to simulate how changes in the flow characteristics will affect the dryer performance, where the simulation for 0,1 m/s results in a laminar air flow in both the collector and dryer while the other four simulations are resulting in turbulent flows.
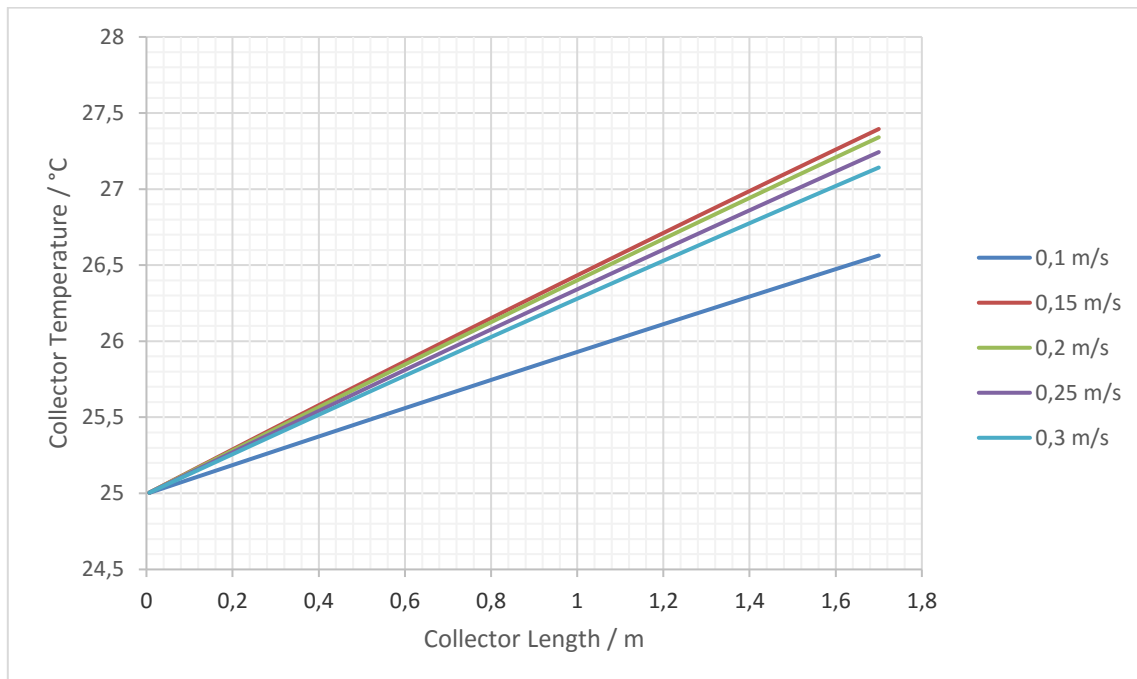

Figure 10 *Calculated air temperatures for the collector modelled in the base scenario. The figure shows how the temperature changes from the inlet to the outlet of the collector for five different air flow velocities.*

The dryer results have been divided into three parts for the base scenario which can be found in Figure 11, Figure 12 and Figure 13. The three figures are showing how the dryer air temperature changes when flowing upwards through the dryer as well as how the relative humidity and drying

rate is affected. Note that the velocities found in the figures are the collector entrance velocities rather than the dryer velocity. The actual dryer velocity will differ from the collector velocity depending on the relation between the collector and dryer geometries, which means for the base scenario that the air velocity is lower in the dryer than it is in the collector.
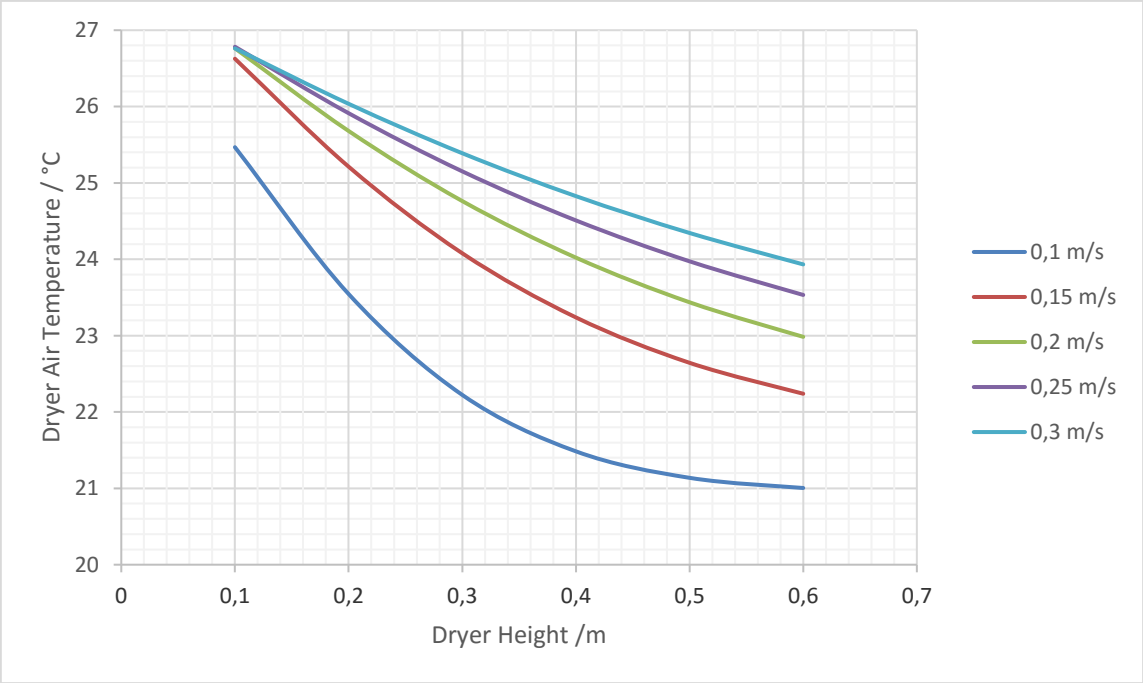

Figure 11   Calculated air temperatures for the dryer modelled in the base scenario. The figure shows how the temperature changes from the first to the last shelf of the dryer for five different air flow velocities of the collector.
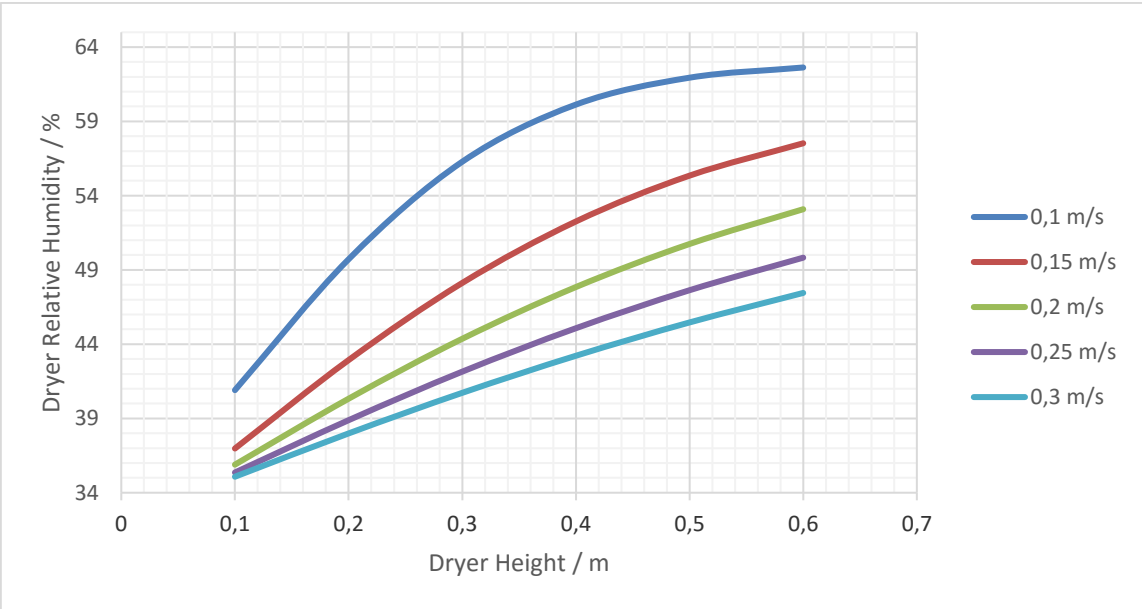

Figure 12   Calculated change in relative humidity for the dryer modelled in the base scenario. The figure shows how the relative humidity changes from the first to the last shelf of the dryer for five different air flow velocities of the collector.
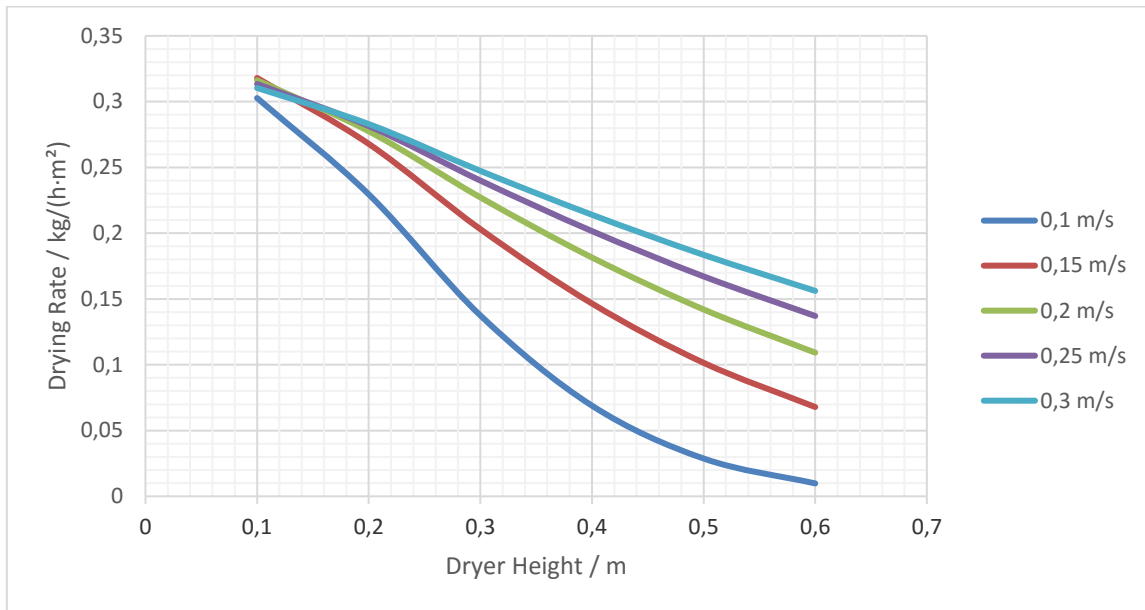
Figure 13   *Calculated change in drying rate for the dryer modelled in the base scenario. The figure shows how the drying rate changes from the first to the last shelf of the dryer for five different air flow velocities of the collector.*

4.2 The collector

The following simulations were carried out as a brief study of what parameters that affect the solar collector the most. To limit the study, results are shown for variations in emittance, the convective heat transfer coefficient and the relation between the width and the height of the cross section. All simulations are performed for the base case with an air velocity of 0,2 m/s.

The first results can be found in Figure 14, where the collector air temperatures have been simulated for five different emissivities. In the base scenario the emissivity was set to a rather high value since low-emittance materials are generally more expensive and difficult to manufacture. On the other hand, if the collector performance would increase greatly by installing low-emittance absorbers this could prove to be a feasible solution.
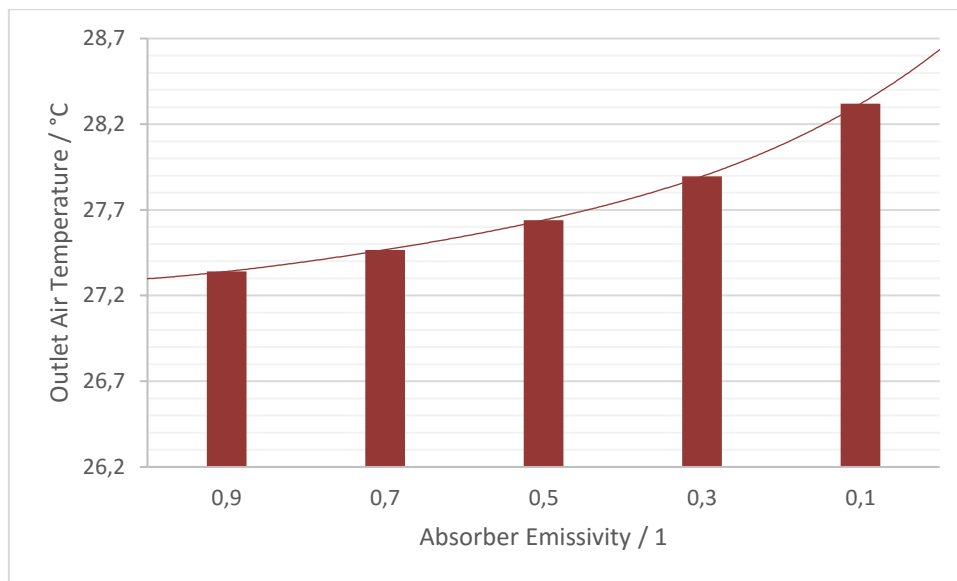

Figure 14 Calculated outlet temperatures of the collector for the base scenario for different absorber emissivities.

In Figure 15 the convective heat transfer coefficient has been changed for the absorber. In practice this could as an example mean that fins have been added to the absorber plate to increase the contact area with the air according to Figure 26, increasing the heat transfer to the air. Note that only the convective heat transfer coefficient for the absorber has been changed, the convection towards the glass and walls are unchanged (see the first term of equation (9) and the second term of equation (14)).
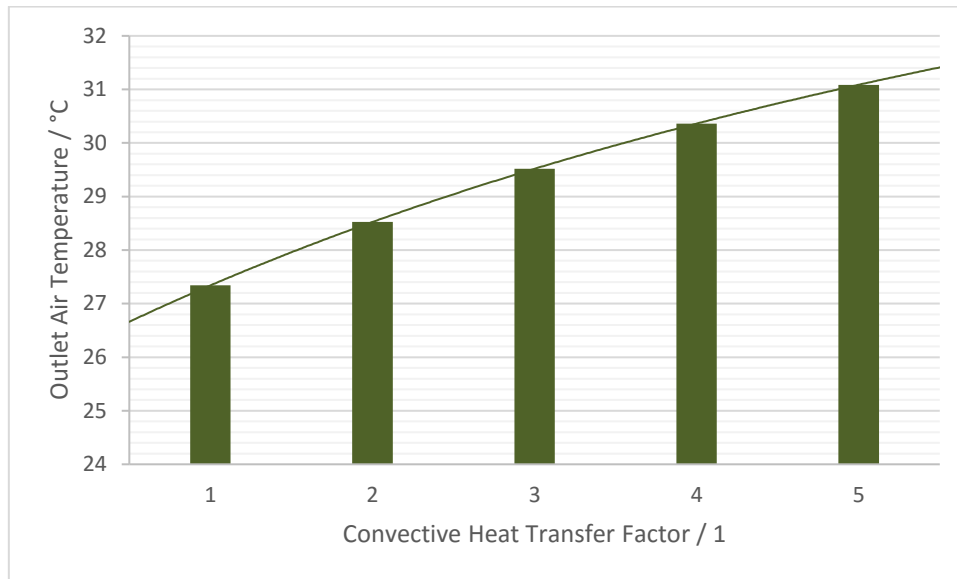
26

Figure 15   *Calculated outlet temperatures of the collector for the base scenario for different convective heat transfer coefficient factors of the absorber.*

The results for the relation between the absorber width and height can be found in Figure 16. Even if the geometry of the collector cross section has been changed, the cross section area is set to a constant value for all simulations of 13,2 dm². This means that the volumetric air flow through the solar dryer is constant for all plotted values.
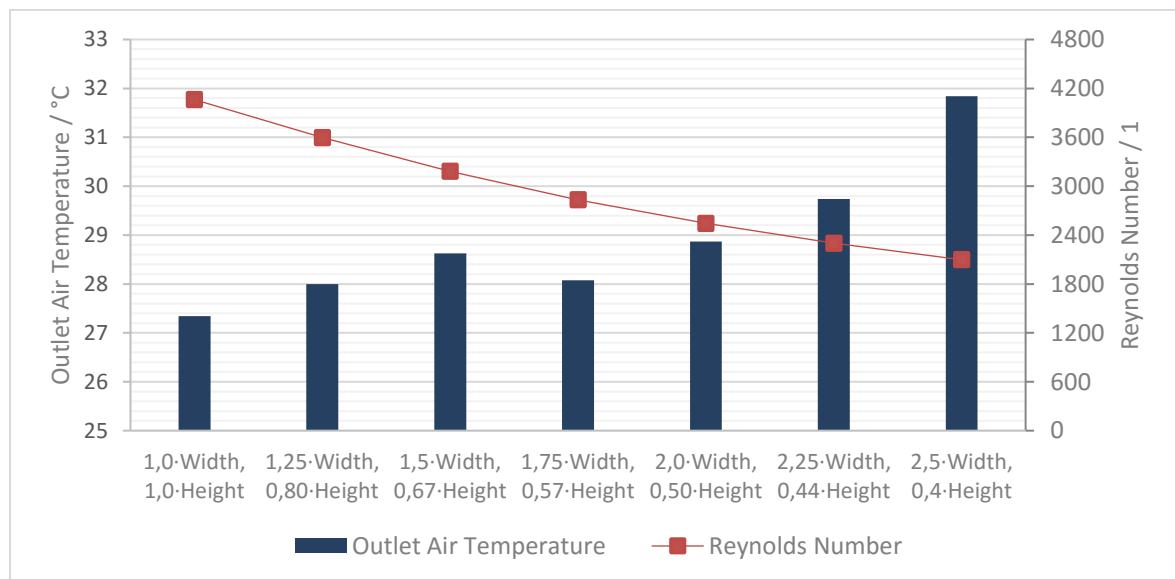

Figure 16   *Calculated outlet temperatures and Reynolds numbers of the collector for the base scenario for different ratios between the width and height of the collector. The ratios have been selected to maintain a constant cross section area.*

In Figure 16 the volumetric air flow was kept constant by keeping the cross section area of the collector constant, but it would also be possible to maintain a constant volumetric air flow if the collector height is decreased while the air velocity is increased. This means that unlike Figure 16, the absorber area is also constant. The results for decreasing the height while increasing the air velocity can be found in Figure 17.
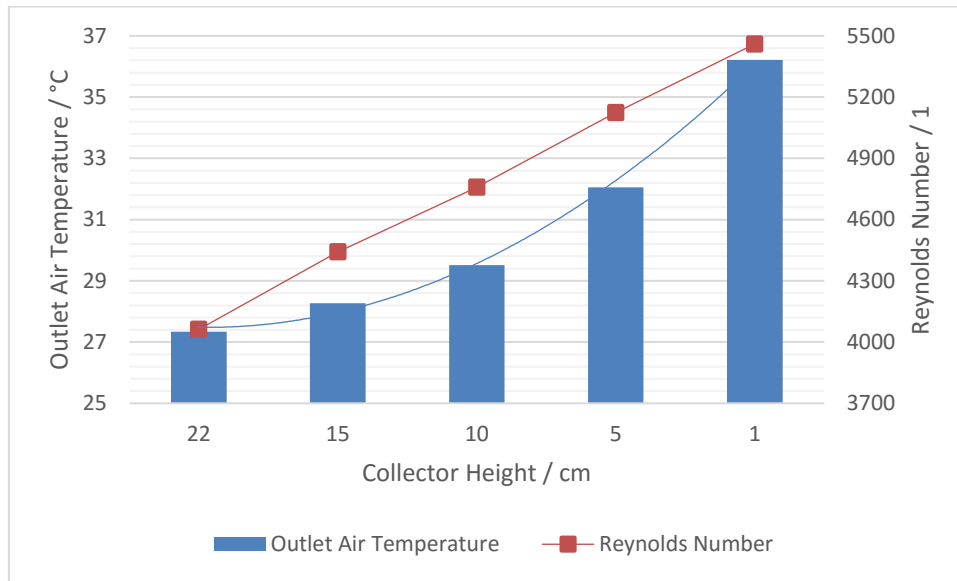
27

Figure 17   Calculated outlet temperatures and Reynolds numbers of the collector for the base scenario for different heights. The air velocity has been adjusted to generate a volumetric air flow of 26,4 liters per second for all selected heights.

Another parameter of interest would be the insulation thickness. For high insulation thicknesses, low lambdas or both, further adding of insulation material would only be redundant for the collector. The results for running simulations for the base scenario for different insulation thicknesses can be found in Figure 18, where the plotted insulation thicknesses have been set for both the collector bottom and sides. The insulation materials remain the same, plywood for the sides and 50 % plywood and 50 % styrofoam for the bottom.
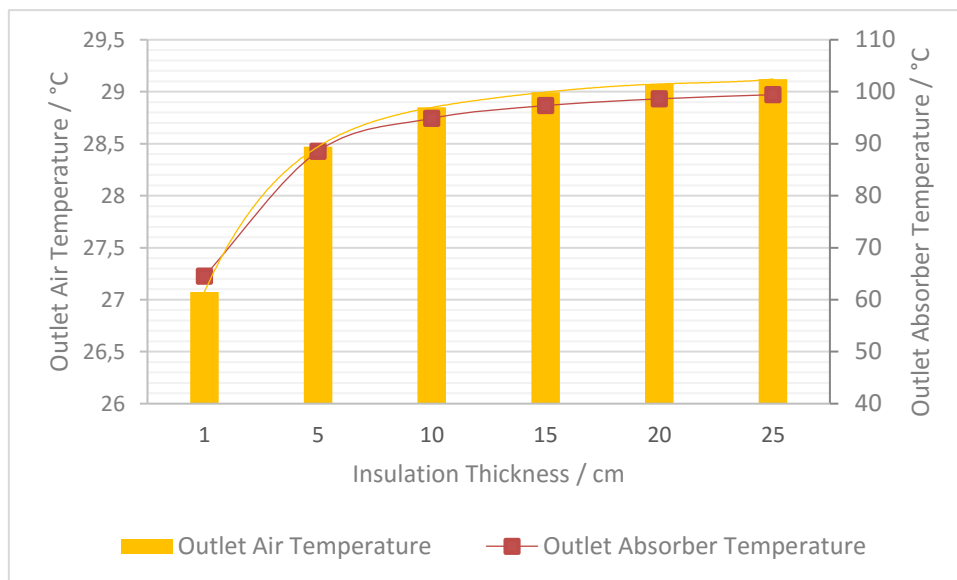

Figure 18   Calculated outlet temperatures for the air and the absorber of the collector for the base scenario for different insulation thicknesses. Note that the insulation thickness has been applied to both the collector sides and bottom.

From the results found in Figure 10 it is worth noticing that the collector air temperature doesn't stabilize over the collector length, meaning that the collector isn't used to its full potential in terms of temperature. In Figure 19 the air flow was reduced significantly to a

velocity of 1 mm/s (or 0,132 l/s) to see what happens when the collector is capable of reaching the stagnation temperature. The stagnation temperature of the air was calculated to approximately 53 °C when the air flow was set to 0 m/s.
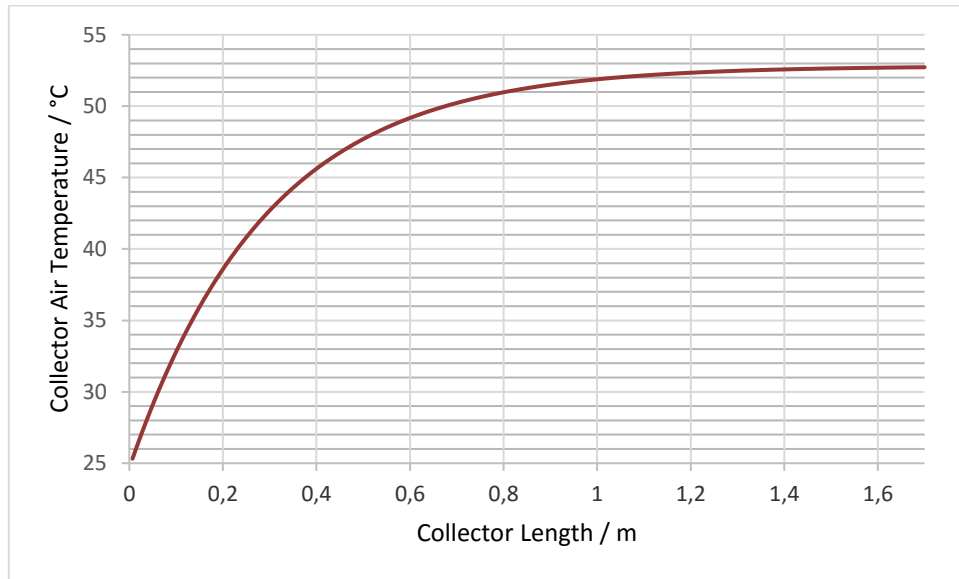

Calculated air temperatures for the collector modelled in the base scenario. The air flow velocity has been reduced to 1 mm/s to allow the air temperature to stabilize.

To check the total energy balance of the collector and highlight the magnitude of the energy losses, the heat losses from the glass and the outer sides and bottom of the collector were summed up for all sections. The result can be found in Figure 20.
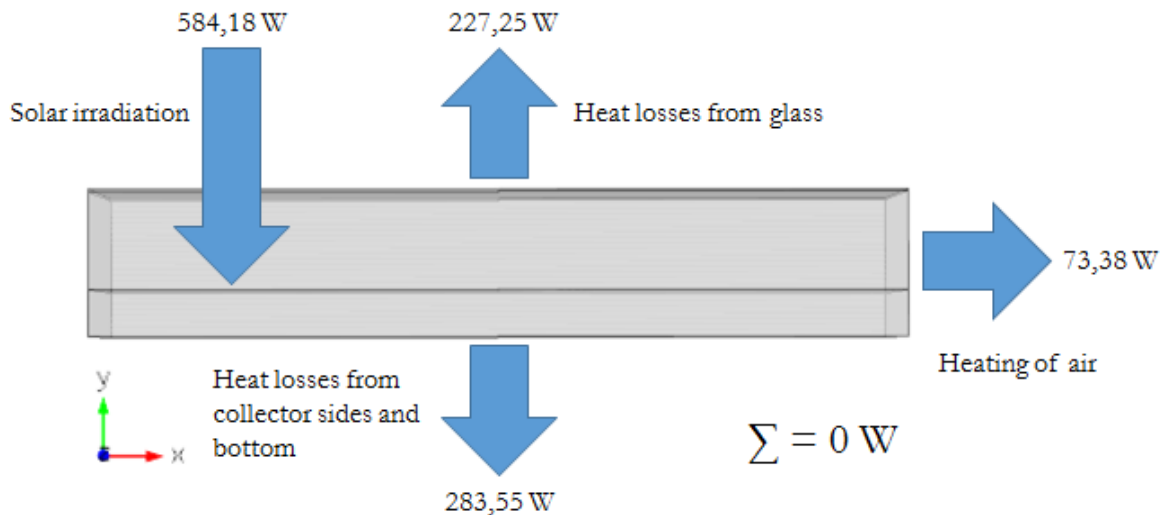

Figure 20 *Schematic figure of the general energy flows of the collector. The values used for the heat transfer coefficients are the average values for the collector length.*

29

4.3   The dryer

Since the intervals of the provided measurements for the drying rate are rather limited, it is very likely that the equation used for determining the drying rate (m_{bags}) will need to be significantly extrapolated, which could generate an error in the simulations. To determine the severity of this error, the drying rate has been multiplied by a factor y ranging from 0 to 2 in Figure 21. Note that the factor y could also be regarded as a parameter for the number of bags placed inside the dryer, since doubling the water mass flux from all bags yields exactly the same result as placing twice as many bags inside the dryer, see equation (23). Apart from the factor y, all parameters are according to the base scenario.
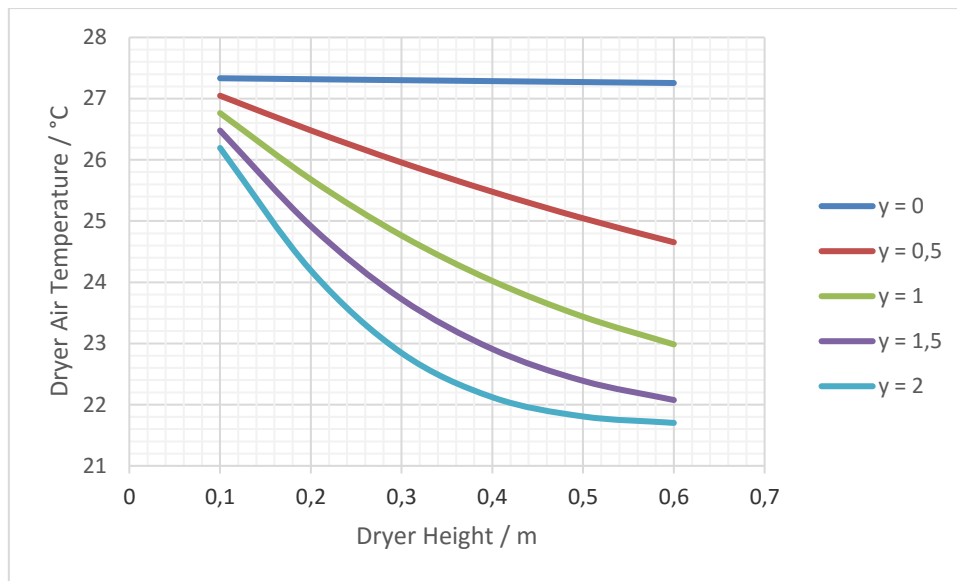

Figure 21   *Calculated dryer air temperatures for different evaporation rates from the SAP-pouches. The value y represents the factor which the mass flow m_{vap} of the base scenario was multiplied with.*

The dryer itself could be used as an additional absorber to heat up the air inside the dryer even further. As an example, if the dryer would be painted black and placed in direct sunlight this would increase the outer wall temperature of the dryer, creating additional heat gains for the air flow. To simulate this effect, the dryer air temperature has been plotted in Figure 22 for five different additional heat gains z (W/m²) on the outer walls of the dryer, see equation (20). Note that the values for z are average values for all four of the collector walls. In reality only one or two sides of the dryer will obtain the majority of the additional heat gains since these are affected by direct sunlight. Also note that 800 W/m² is a very high value, which would require mirrors to irradiate all four outer sides of the dryer as well as concentrating the radiation.
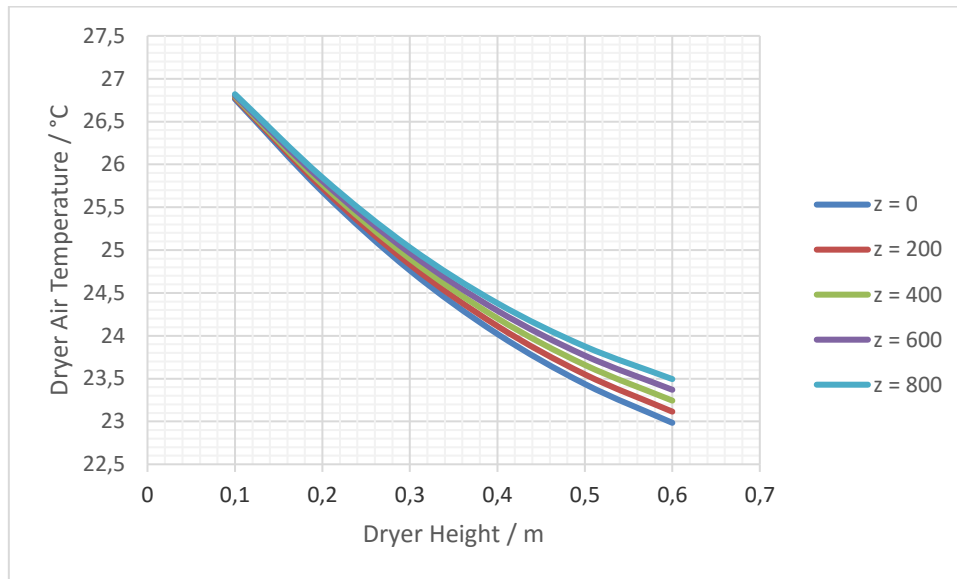
30

Figure 22   Calculated dryer air temperatures for different additional heat gains to the outer wall of the dryer. The value n represents the average heat gain for all four sides of the dryer in W/m².

4.4   Creating a more optimal solar dryer

Judging from the results of the base scenario, there are many different parameters that can be adjusted to create a better drying process. In this section of the report a more optimal solution to the drying process will be presented. Once again the base scenario has been used, but this time with changes to multiple parameters. The parameters changed can be found in Table 5 and the results are presented in Figure 23.

Table 5   A summary of all changed parameters of the base scenario to create a more optimal solar dryer.

Changed Base Scenario Parameter	Value	Unit
Collector Width	1,2	m
Collector Height	0,05	m
Collector Length	2	m
Dryer Width	0,2	m
Dryer Length	0,2	m
Collector Side Insulation Thickness	0,1	m
Collector Bottom Insulation Thickness	0,1	m
Collector Convective Heat Transfer Coefficient Factor	2	1
λ_{side} (Collector)	0,035	W/(m·K)
λ_{bottom} (Collector)	0,035	W/(m·K)
Additional Heat Gains to Dryer	400	W/m²
SAP-Pouches per shelf	2	1
Number of Shelves in Dryer	8	1

The parameters that are not presented in Table 5 will remain according to Table 1, Table 2, Table, 3 and Table 4. Note that the collector convective heat transfer coefficient has only

31

been adjusted for the absorber so simulate the effect of adding fins to the absorber plate in a similar manner as the results found in Figure 15.

After entering the new parameters found in Table 5 into the model, the results found in Figure 23 could be obtained. The upper left graph of Figure 23 represents the temperature increase of the air flow from the inlet to the outlet of the collector, similar to Figure 10. The upper right graph represents temperature increase of from the inlet to the outlet of the dryer, which can be compared with Figure 11. The bottom left graph shows the change in relative humidity from the inlet to the outlet of the dryer in a similar way as Figure 12 did for the base scenario. The fourth graph in the bottom right corner shows the change in drying rate of the SAP-pouches from the inlet to the outlet of the dryer in a similar way as Figure 13 does for the base scenario. Note the changed values of the y-axis for the figures.
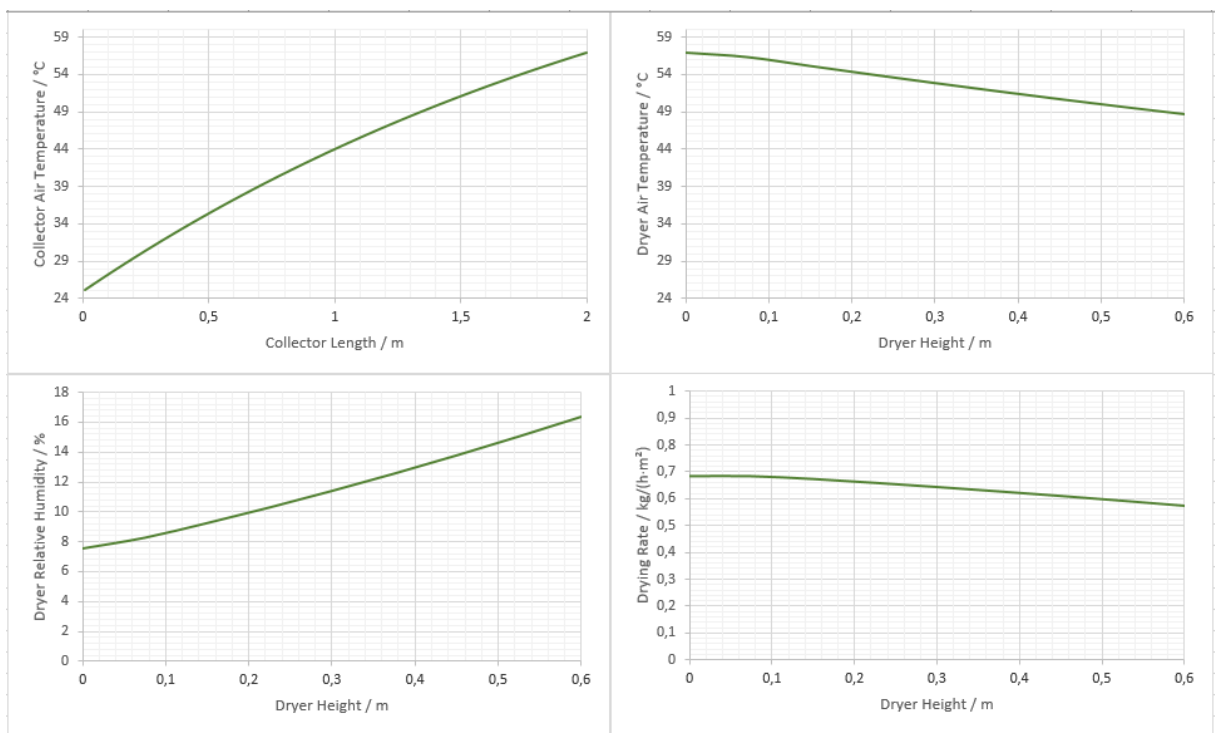

Figure 23   *Results from the improved version of the base scenario. The calculated collector air temperature can be found in the upper left figure and the remaining figures show the results for the dryer air temperature, relative humidity and drying rate.*

4.5   Control calculations for approximations

4.5.1 Additional heat gains of the dryer

In the results section in Figure 22 the effects of additional heat gains to the dryer were studied to simulate how significant the change in the dryer air temperature would be if the dryer would be exposed to sunlight. In practice the solar dryer will be placed in a sunny spot where both the collector and dryer will be exposed to solar radiation, resulting in both the collector and the outer walls of the dryer being heated up. This means that the heat losses from the dryer walls in the model will be reduced or even turned into a heat gain if the irradiation is high enough. However, the dryer walls won't be able to heat up as efficient as the collector will since the outer walls aren't covered by a layer of glass. The convective heat transfer coefficient on the outside of the dryer was set to a rather high constant value of 20 W/(m²·K), meaning that a significant part of the heat on the outer wall will be transferred to the ambient air. In other words, the additional heat gain isn't as effective as it would be in the collector. This effect is shown rather well in Figure 22, since increasing the additional heat gain with 800 W/m² only appears to increase the dryer air temperature by 0,5 °C. Note that an average value of 800 W/m² is a very extreme value which could only be achieved if mirrors are placed around the dryer to reflect sunlight to the sides which aren't exposed to direct sunlight. But nevertheless, it is an increase and thus an improvement.

The effects of additional heat gains could be amplified if the dryer was to be designed differently. Unlike the collector, where it is important to keep the heat from going through the walls and bottom, the opposite would appear to be preferable for the dryer. If the dryer was to be painted black on the outside in order to be used as an additional heat source for the dryer air flow, it would be more beneficial to have as little insulation as possible, at least for the irradiated sides of the dryer. This would improve the heat transfer from the outer to the inner walls of the dryer since the U-value would be higher and consequently increase the dryer air temperature. As seen in Figure 20, the vast majority of heat losses of the dryer occurs from water evaporation from the SAP-pouches. When n is set to 0 in Figure 21 only the heat losses from the walls of the dryer will remain and since the temperature difference between the dryer air flow and the ambiance is low, the heat losses through the side insulation are nearly negligible.

In the results found in Figure 22, the additional heat gains plotted were assumed to be the average heat gains for all four of the dryer sides. As discussed earlier, it is a lot more likely that just one side is exposed to 800 W/m² than all four sides being exposed to 200 W/m². If the dryer would have a square cross section, the average heat gains for both cases would be 200 W/m² but at the same time the outer wall temperatures would be very different. Since the radiative heat transfer coefficients are temperature dependent, see equation (17) and (18), it is possible that this approximation would give an inaccurate result. In order to control how big the difference would be for the two described cases, calculations were made for the heat transfer between the outer and inner walls of the dryer. The total heat transfer one outer wall being exposed to 800 W/m² was added with the heat losses from three walls without additional heat gains and compared with the total heat transfer of four walls with 200 W/m²

heat gains. The results can be found in Table 6, where the dryer wall temperatures were obtained after running simulations for the selected heat gains.

Table 3   *A comparison between two ways of using additional heat gains of the dryer in the model. The energy flow from the outer side of the dryer wall to the inner side of the dryer wall was calculated for 0 W/m², 800 W/m² and 200 W/m² additional heat gains. In the lower section of the table the energy sum of three walls exposed to 0 W/m² and one side exposed to 800 W/m² was compared with the sum of four walls being exposed to 200 W/m².*

	0 W/m²	800 W/m²	200 W/m²	Unit
$T_{wall,out}$	296,25	326,19	303,92	K
$T_{wall,in}$	296,32	324,96	303,66	K
λ_{wall}/t_{sides}	13	13	13	W/m²·K
A_{side}	0,3	0,3	0,3	m²
E_{side}	-0,7621	4,779	1,035	W
E_{tot}	4,017		4,142	W
Diff.	0,1255			W

As shown in Table 6, the approximation to use an average value for the additional heat gains does result in a higher value. The reason for the difference is due to the much higher outer wall temperature for the case with 800 W/m² on one side. A wall with a higher surface temperature will have a higher radiative heat transfer coefficient which results in higher heat losses. On the other hand, the 0,13 W difference between the cases could be regarded as a negligible error since it would only result in a 0,004 °C difference in the dryer air temperature if the air velocity remains the same.

But in either case, averaged value or not, it is clear that the additional heat gains are worth considering. The higher the heat gains are the higher the dryer air temperature will be. It could for this reason be relevant to use reflectors to irradiate all four of the dryers sides, paint the sides black and use as little insulation as possible. Whether or not this would be applicable for a developing country like Mozambique would require further studies.

4.5.2 Analysis of the internal convective heat transfer coefficient

The internal convective heat transfer coefficient is one of the most important parameters to consider for the solar collector. Since the air flow cannot absorb any heat radiation, the convective heat transfer will be the only transfer of heat from the absorber to the air. For this reason, it is very important that the calculation methods used for obtaining the convective heat transfer coefficient are accurate. While creating the model in Maple, several different equations were found for calculating the Nusselt number. Even if some of the equations were valid for the same intervals, the calculated Nusselt numbers would differ from equation to equation. This lead to the problem of determining which equation to use in the model.

In Figure 24 the Nusselt number has been plotted as a function of the Reynolds number for three different equations used for turbulent flows valid for Re ≥ 3000 as well as the highest and lowest possible Nusselt numbers for fully developed laminar flows. Eq 1 found in Figure 24 is the equation used in the model to determine the Nusselt number (see equation (5)). Eq 2 is a rather similar expression to Eq 1, since both equations are taking the friction factor of

the surrounding walls into account (see equation (6)), but Eq 2 is not valid for Re > 10^4 unlike Eq 1 (Incropera & Dewitt, 2002). Eq 3 is a more general equation used for turbulent flows and is considered to be valid for Re ≥ 2100, but doesn't include the friction factor (Department of Chemical Engineering of Lund University, 2013).
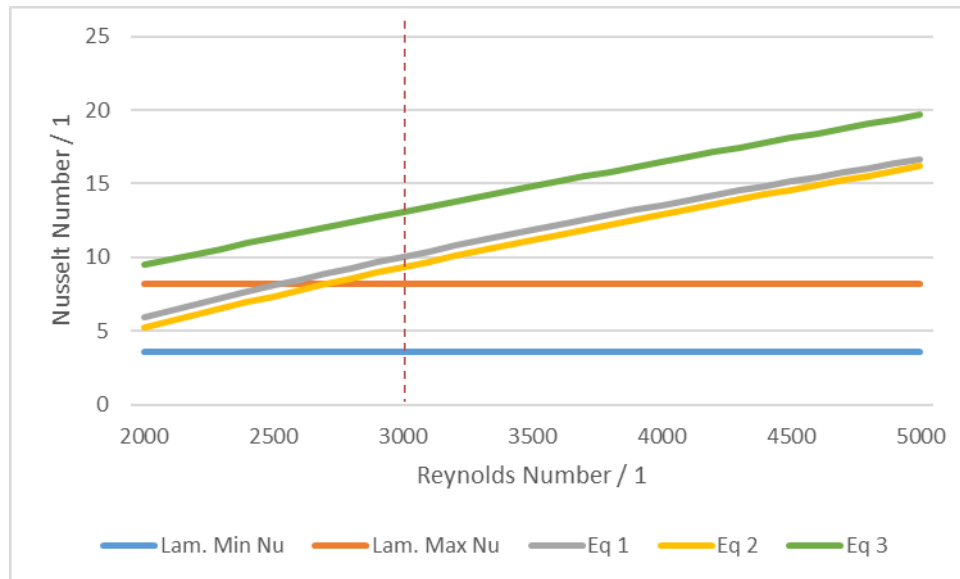

Figure 24   *Comparison of the Nusselt number calculated for different Reynolds numbers for laminar and turbulent flows, where the dotted line indicates where the flow becomes turbulent (Re = 3000). For the laminar flows the lowest and highest values are plotted. For the three turbulent flow graphs Eq 1 represents the equation (5), Eq 2 represents an alternative version of equation (5) and Eq 3 represents an equation independent of the friction factor.*

For lower values of the Reynolds number the difference between Eq 1 and Eq 2 are very marginal, but Eq 3 will always yield a significantly higher value for the Nusselt number. It is worth mentioning that most models used for calculating the Nusselt number have been approximated from empirical studies, normally studying long and thin metal pipes with flowing water inside. In other words, the conditions for a solar collector are very different compared with the scenarios from which the equations originated from. This could mean that another method for determining the Nusselt number is necessary to find a more accurate value.

Another thing worth observing in Figure 24 is how the model built in Maple works practically. When the Reynolds number is below 3000, the air flow is assumed to be a fully developed laminar flow. Depending on the ratio between the height and the width of the collector, the Nusselt number will be selected to a constant value ranging between 3,61-8,23. When the Reynolds number reaches 3000 the model will instead use equation (5) to determine the Nusselt number for a turbulent flow, resulting in in a distinct jump in the graph. This jump occurs due to the assumption made that the flow will either be fully developed and laminar or fully developed and turbulent, but in reality there is an interval for a developing turbulent flow before the flow becomes entirely turbulent. In this regard there are improvements that can be made to the model built in Maple, and it could be relevant to look further into the flow characteristics of the solar dryer. Since the collector is relatively short and has a large cross section compared with a thin metal pipe, the entrance length will be long. A long entrance length means that the flow will require a longer distance to become

35

fully developed, which in turn means that the flow characteristics will vary from the inlet to the outlet (Incropera & Dewitt, 2002). Taking into consideration that the flow characteristics will determine how much heat that is transferred from the absorber to the air, it could be worth making practical measurements of the convective heat transfer coefficient of a solar collector.

4.5.3 Error analysis of the approximations for the collector sides

To simplify the model, the temperature of the inner sides of the collector were assumed to be the mean value of the absorber and glass temperatures. If the model was to be made more accurate, a fifth energy balance would be required to describe the conditions for the sides since a fifth variable temperature would be added into the equations. However, the effects of the walls of the collector appear to have a very minor influence on the collector temperatures, which is shown in Figure 25.
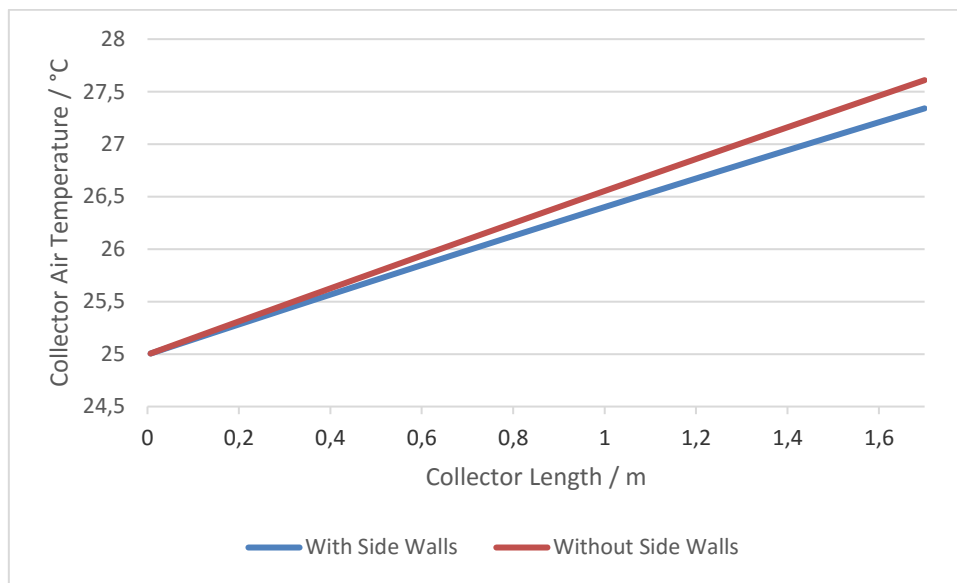

Figure 25   Comparison for the collector temperature of the base scenario with and without mathematical expressions for the collector sides.

To remove the sides of the collector in the simulations, A_{sides} was set to 0 for equation (9) for the collector air flow, equation (14) for the absorber and inner sides and equation (16) for the outer walls. Figure 25 shows that the walls cause a approximately 10 % temperature drop at the outlet of the collector, which can be considered rather reasonable since the side areas of the collector were rather large and had a thin layer of insulatin in the base scenario. Since the majority of the heat losses appears to be at the bottom and the glass of the collector, the heat losses from the sides of the collector will be close to negligible for a flatter and more well insulated collector, e.g. the more optimal scenario. This means that the flatter the design of the collector, the less the approximation will matter and even for relatively high collectors at 22 cm the side losses are very small.

5 Discussion

After entering the selected parameters for the base scenario into the program built in Maple the theoretical values were calculated for the absorber, outer wall, glass- and air temperatures of the collector as well as the air, inner- and outer wall temperatures for the dryer. To obtain a better understanding of the drying process of the SAP-pouches, the dryer relative humidity and drying rate were also calculated. The base scenario was set up according to an experimental dryer which was tested in a laboratory environment and had about the same appearance as the solar dryer found on the cover page of this report. Yet theoretically, this design appears to be far from optimal. In this section of the report the base scenario will be analyzed to find methods of creating a more optimal solar dryer based on the results of the report.

5.1   High collector air velocities and low dryer air velocities

The collector temperatures, which can be found plotted in Figure 10, reveals that the selected collector design is inadequate to yield the desired air temperature of 50-65 °C to maintain a sterile drying process and maintain nutrients. One of the reasons for the outlet temperature being just below 28 °C is the air flow velocity, which is rather high at 0,2 m/s (or approximately 26 liters per second). This means that the residence time for the air molecules inside the collector is only 8,5 seconds. The reason for wanting a high air flow can be found in equation 23 for the evaporation rate, where a higher air velocity surrounding the SAP-pouches will increase the evaporation rate. And this is where the main problem with the base scenario comes into play; the air velocity inside the collector is higher than in the dryer. The function of the collector is to raise the air temperature, but in order to do so the flow must be as low as possible. As shown in Figure 19 the highest possible temperature of the collector is the stagnation temperature, which is only achieved if the air flow is very low or if there is no flow at all. This contradicts the conditions for the dryer, where the flow needs to be as high as possible. If the flow inside the dryer is low, the SAP-pouches will have a slower evaporation rate according to equation (23). In addition to this, the concentration of water in the air will be higher which increases the relative humidity. The worst effect of the increased relative humidity at slow air velocities is that the relative humidity will be much higher at the last shelf compared with the first shelf (see Figure 13), which will be discussed further in the following sections.

5.2   Absorber fins could increase the convective heat transfer

Even if the maximum temperature of the dryer would be achieved through stagnation, the convective heat transfer from the absorber plate to the air would be higher with a higher air velocity. The convective heat transfer coefficient of the absorber is one of the most important parameters of the entire collector, since this will determine how much heat that is transferred to the air. As seen in Figure 10, the collector outlet temperature decreases drastically when the air flow is below 0,15 m/s. The reason for this is because between 0,15

m/s to 0,1 m/s the air flow becomes laminar and laminar air flow has a much lower convective heat transfer coefficient than a turbulent flow.

Having mentioned this, there are other ways to increase the convective heat transfer than increasing the air flow. In Figure 15 an attempt has been made to simulate the addition of fins to the absorber plate, which has been illustrated in the left side picture of Figure 26 below.
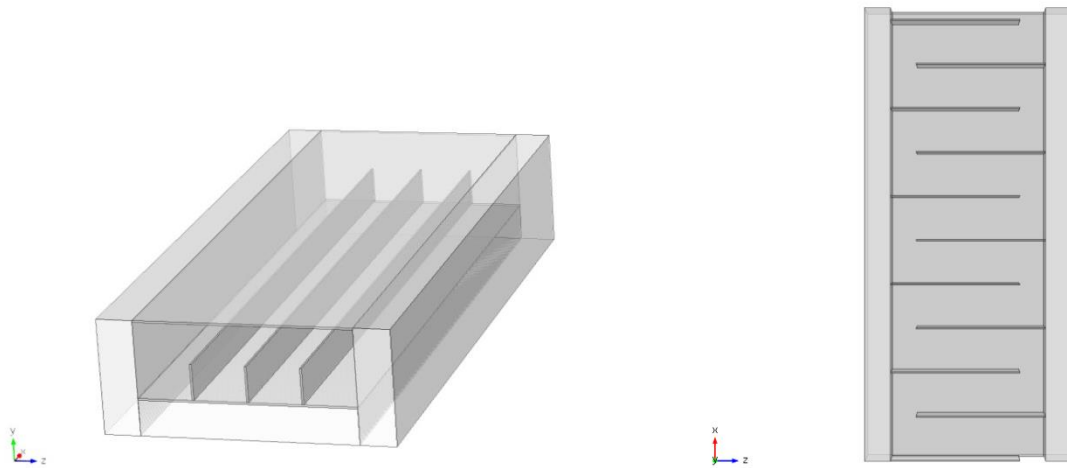

Figure 26   *Two ways of adding fins to the collector. Left figure: parallel fins placed on top on the collector. Right figure: Fins have been placed sideways along the collector to partially obstruct the air flow, forcing it to change direction.*

By adding parallel fins to the absorber, the contact area between the air and the absorber would be increased and thus increase the convective heat transfer. As shown in Figure 15, the higher the convective heat transfer is the higher the outlet temperature will be. On the other hand, if the collector would be designed to create a meandering air flow from the inlet to the outlet according to the right side picture of Figure 26 the air flow would be forced through a narrower passage. This would increase the velocity and make the flow more turbulent. In other words, the collector cross section area would remain the same, but the effective cross section area for the air flow would be decreased. But there is one significant disadvantage with this design compared with the parallel fins and that is that the convective heat transfer coefficient will increase for both the absorber and the glass. The increased velocity will increase the heat transfer rate from the absorber to the glass, but at the same time the heat losses of the glass would increase since more heat is transferred to the glass as well. Both designs would most likely increase the air temperature compared with the base scenario. Perhaps a combination of both would be the best solution.

5.3   Improving the collector insulation would help – to a degree

In Figure 18 the results for running simulations of the base scenario can be found for different insulation thicknesses. It is quite clear that improvements of a thinly insulated collector will yield significant increase in temperature, but at one point adding more insulation will have nearly no effect. This is worth considering, especially for a developing country since more insulation means higher material costs.

In the base scenario, the side insulation consists of 1 cm of plywood and the bottom insulation consists of 1 cm of plywood and 1 cm of styrofoam. It is made apparent by Figure 18 that these thicknesses are inadequate, since an increase to 5 cm of side and bottom insulation would improve the temperature of the collector significantly. On the other hand, one might wonder why more insulation isn't always better for the collector since the majority of the heat losses appears to occur at the bottom and sides of the collector according to Figure 20. If the insulation thickness would be 15 cm, adding another 10 cm of insulation would have nearly no effect on the collector air temperature. The explanation to this is that the absorber temperature will increase if the bottom and sides are more well insulated, which increases the radiative heat transfer from the absorber to the glass. According to Figure 18, the absorber temperature was calculated to 64,5 °C for 1 cm of side and bottom insulation while increasing the insulation thickness to 25 cm resulted in an absorber temperature of 99,4 °C. This will mean that more heat will be transferred to the air flow, but at the same time the temperature difference between the absorber plate and the glass will be much higher. While the heat losses from the bottom and sides have been nearly eliminated due to the thick layer of insulation the heat losses of the glass layer are increased, leaving little additional heat for the air flow. For this reason alone, it could be relevant to study if multiple glass layers would be a feasible option for the dryers used in Mozambique.

5.4   A flatter collector is likely to increase the performance

The initial idea of creating a flat collector was to increase the contact area of the air and the absorber as well as adding more solar energy to the collector by increasing the size of the absorber. Increasing the size of the absorber is only a problem if costly materials are used, but in the base scenario the absorber parameters are selected to simulate a black painted plywood board which can be considered a cheap material.

In Figure 16 the dimensions of the cross section area were changed according to the graph. It is important to remember that the volumetric flow for all values in Figure 16 are equal, which basically results in a comparison of the collector efficiency. Up to the third value from the left of the graph, the temperature unsurprisingly increased. But after the third value, the temperature actually decreases before it starts to rise again. This can be explained by the flow characteristics of the collector, as increasing the width from 1,5 times to 1,75 times the base values and decreasing the height from 0,67 to 0,57 times the base value results in the Reynolds number dropping below 3000. What this means for the model is that equation (5) which is used to calculate the Nusselt number for a turbulent flow is replaced with a constant, lower Nusselt number according to Appendix B. The reason for the Reynolds number to decrease with a flatter cross section area can be found in equation (8) for calculating the hydraulic diameter of the collector, which is directly proportional to the Reynolds number. If the width is increased and the height is decreased, the hydraulic diameter will decrease, resulting in a lower Reynolds number. Even if the assumptions are made that turbulence only occurs at Re ≥ 3000 and for lower values the flow is fully developed, it can be worth considering what kind of flow that will occur in the collector. Turbulent flows result in a better heat transfer which is preferable and at some point making the collector flatter can actually decrease the performance. It is worth noting that the sudden temperature decrease in

Figure 16 occurs due to a change in calculation methods for the convective heat transfer coefficient. In this regard the temperature drop could be exaggerated and further development of the model would be recommended to find smoother transitions for the Reynolds numbers.

Yet in general it appears that the collector should be designed as flat as possible, even if the flow will become laminar. The downside of adjusting the collector according to Figure 16 is that the absorber area must be increased since the width is increased, which increases the amount of materials required to build the collector. This would become particularly problematic if the absorber would consist of costly materials. An alternative method of making the collector flatter while maintaining the same volumetric air flow would be to decrease the height and increase the air velocity. This would reduce the required amount of materials needed to build the collector since the sides will be made shorter while the absorber area will remain unchanged, which was not the case for Figure 16. As shown in Figure 17, it appears to be more efficient to make the collector flatter by decreasing the height and increasing the air velocity than adjusting the cross section area according to Figure 16. The reason for this can be found in Figure 16 and 17 when looking at the Reynolds numbers for the two cases. As discussed earlier the Reynolds number for a flatter collector according to Figure 16 will decrease the flatter the collector becomes. However, this is not the case for Figure 17, as the increased velocity will have a greater effect on the Reynolds number than the decrease in hydraulic diameter. Increasing the air velocity will increase the Reynolds number, which causes the air flow to become more turbulent and thus the convective heat transfer is increased. In other words, less materials are used and higher temperatures are reached compared with Figure 16, but the downside is that the air velocity must be increased significantly. To maintain the same volumetric air flow in Figure 17, a collector height of 1 cm would require an air velocity of 4,4 m/s. It is hard to imagine such high air velocities generated through natural convection, which means that fans would almost certainly be a requirement.

5.5   Low emittance absorbers are effective, but not required

As shown in Figure 14 the lower the emittance of the absorber is the higher the temperature will be. It is also worth noticing that the curve appears to be exponential, meaning that high temperature increases will only be achieved for the lowest selection of emissivity values. In other words, it's questionable if a marginally better absorber would justify the increased material costs since the low emittance materials are likely to be more costly. This means that the most efficient way of selecting the absorber is to select the one with the lowest emittance.

On the other hand, a low emittance absorber may not be required at all. Looking into the results found in Figure 23 for the more optimal solar dryer, the temperature of the dryer seems to range between 56,9-48,7 °C which can be considered an acceptable temperature interval for a sterile drying process while preserving nutrients. Note that this temperature interval has been reached with an absorber emittance of 0,9 and that the solar irradiation was set to 700 W/m², which is probably lower than it will be in Mozambique. By optimizing other parameters of the solar dryer, high temperatures can be reached without the use of complex and costly materials.

40

5.6   The number of SAP-pouches exceeds the dryer capacity

Before discussing the dryer capacity for SAP-pouches, it is worth reminding that the measurements used to find an expression for the evaporation rate of the SAP-pouches (m_{vap}) were provided in the wrong intervals for relative humidity and air velocity. The values provided are plotted in Figure 8 and the expression for m_{vap} (equation (23)) was extrapolated for these values. To create a more exact expression a more extensive study will be required where the measurements are made in a more suitable interval for relative humidity, air velocity and temperature.

Regardless of the accuracy of the expression, this study has not been performed to generate exact values but rather to find trends and correlations between different parameters. In Figure 21 the evaporation rate of the SAP-pouches was modified by adding a factor n to m_{vap}. The dryer contained 6 shelves, each holding 10 pouches for drying. Since the air flow of the base scenario was low, more water was able to accumulate in the air traversing the dryer. This resulted in a significant variation in drying rate from the first to the last shelf of the dryer. But even if the air flow were to be adjusted, which is illustrated in Figure 13, the high variations in drying rate would remain since an increased air velocity will also increase the evaporation rate according to equation (23). What this basically means is that the dryer modelled in the base scenario containing a total of 60 SAP-pouches was exceeding the capacity for how many bags that could be dried simultaneously. In the more optimal scenario this problem has been considered and the total number of bags was reduced to 16. This resulted in a much more homogenous drying rate through the entire dryer, as shown in Figure 23. The more optimal scenario had 8 shelves holding 2 pouches each. It would have been more optimal regarding a homogenous drying rate to place all pouches on the same shelf, but since the dryer cross section was designed to be narrow only two pouches could be fitted on a shelf.

The dryer and collector of the base scenario holding 60 pouches could be redesigned to handle such high capacities of pouches, but this would require several rather extreme changes to the design. The temperature of the air flow as well as the air velocity would need to be increased significantly, which would have to be solved by creating a more efficient and larger collector. Drying as much as 60 pouches simultaneously without changing the design will only result in the pouches placed on the last shelves being left undried. It is for this reason very important to consider the capacity of a collector, unless manually rearranging the SAP-pouches is considered an option. Having just a single shelf would solve the problem with variations in drying rate entirely, but would result in a much larger cross section area of the dryer in order to fit all the bags which in turn would slow down the air velocity.

41

6 Conclusion

The program built in Maple resulted in a sufficient calculation tool for calculating various temperatures and the drying rate of an indirect solar dryer. The results are not generated to find exact values, but rather to find out the general effects of various parameters. Judging from the results of the simulations made in the program, the following conclusions have been made:

- A solar dryer designed according to the base scenario of this report is not the optimal way of constructing an indirect solar dryer.
- The proportions of the solar dryer are very important to consider. If the collector is to be designed rather high and for a high air flow the collector is likely to generate very low temperatures. The highest possible temperature of the collector is the stagnation temperature, meaning that the flow should be as low as possible. The opposite is valid for the dryer, since a lower air flow generates greater variations in drying rate from shelf to shelf as well as generally slowing down the drying rate.
- Adding fins to the absorber of the collector could be an efficient method to increase the collector outlet temperature.
- Increasing the insulation thickness of the collector is only relevant if the insulation thickness is thin or has low thermal conductivity. For the base scenario, adding more than 10 cm of insulation, representing an average U-value of 0,83 W/(m²·K) for the sides and bottom, is redundant.
- Designing a flatter collector by adjusting the cross section area a greater absorber area is used to heat up the same volumetric flow of air, generally resulting in higher temperatures. However, at one point the flow will change from turbulent to laminar, which decreases the absorber performance. This would not be the problem if height would be reduced and the air velocity would be increased, but this solution is likely to require the installment of a fan.
- Low-emittance absorbers are very efficient for increasing the collector air temperature, but aren't required if other parameters are optimized instead.
- Large numbers of SAP-pouches placed inside the dryer could result in high drying rate variations from one shelf to another. This needs to be considered since a slower drying rate generates a greater risk for the food to become inedible during the drying process. For this reason, it could be relevant to determine the maximum SAP-pouch capacity for specific solar dryer designs.
- To improve the air temperature inside the dryer additional heat gains could be utilized using less insulation and better absorbing outer walls of the dryer. However, the results for the additional heat gains found in this report are highly speculative and further study on the subject is advised.

7 Uncertainties and further development

The values obtained using the program built in Maple have not been verified by any third party control, making it more difficult to draw any conclusion of the accuracy of the program. To solve this problem, suggestions for further development of the model are as follows:

- Comparing the results with other simulation models. One way of doing this would be to create a similar model in COMSOL Multiphysics, which is a well-used program for simulating heat transfer.
- Practical measurements of the convective heat transfer coefficient. The convective heat transfer coefficient was assumed to be a constant value for the external walls of the solar dryer while equation used for the internal walls could prove to be inaccurate for a solar dryer. The convective heat transfer is crucial for making accurate estimations of the collector air temperature and will also determine the majority of the heat losses from the solar dryer. It could also be relevant to measure the convective heat transfer coefficient when fins have been added to the absorber.
- The equation used for the evaporation rate from the SAP-pouches was heavily extrapolated from measurement data. The intervals of the temperature, relative humidity and air velocity of the measurements provided were far off the calculated values, which is very likely to have generated faulty evaporation rates of the dryer in the model. The drying rate is definitely the most important equation of the entire solar dryer since this will determine the drying performance.
- The air flow of the solar dryer is assumed to be constant. To simulate an air flow occurring solely by natural convection the model will have to be remade to include a variable air flow.
- Including equations for the inner side walls of the collector. While this isn't likely to have any greater effect on the collector temperatures, it would still be an improvement.
- A more advanced radiation model. In the created model the radiation from the absorber to the glass is considered only to be vertical but in practice the radiation will spread out across the entire glass.
- Options to add multiple layers of glass and to simulate direct- and hybrid dryers.
- Adding more accurate equations for the Nusselt number for developing turbulent flows would improve the model for intermediate Reynolds numbers (2000 < Re < 3000). The air flow is not likely to become fully developed and laminar for Reynolds numbers slightly below 3000, especially not for short collectors, which will have an effect of the convective heat transfer.
- The model could be improved by implementing usage of weather data for temperature, relative humidity and solar irradiation.

In general, the model needs to be compared with practical measurements where all of the parameters entered in the model are known.

Literature References

Augustus et al. (2002). *A comprehensive procedure for performance evaluation of solar food dryers.* Klong Luang, Thailand: Asian Institute of Technology.

Bratt, C., & Ånger, G. (2015). *Concept Design of Fruit Preservation Product for Mozambican Smallholders.* Lund: Lund University.

Burdurlu et al. (2005). *Degradation of vitamin C in citrus juice concentrates during storage.* Ankara, Turkey: Ankara University.

Department of Chemical Engineering of Lund University. (2013). *Handbook.* Lund: MediaTryck.

Ekechukwua, O., & Norton, B. (1997). *Review of solar-energy drying systems II: an overview of solar drying technology.* Nsukka, Nigeria: University of Nigeria.

Hammar, L. (2011). *Distribution of Wind and Solar Energy Resources in Tanzania and Mozambique.* Gotherburg: Chalmers University of Technology.

Hossain et al. (2008). Hybrid solar dryer for quality dried tomato. *Drying Technology: An International Journal*, 1591-1601.

Incropera, F. P., & Dewitt, D. P. (2002). *Fundamentals of Heat and Mass Transfer.* New York: John Wiley & Sons, Inc.

Kumar et al. (2015). *Progress in solar dryers for drying various commodities.* Hisar, India: Guru Jambheshwar University of Science & Technology.

Kumar Moningi, M. (2016, March 29). *Conduction Convection Radiation processes of a solar collector using FEA.* Retrieved from unix.ecs.umass.edu: http://www-unix.ecs.umass.edu/mie/labs/mda/fea/fealib/moningi/moningiReport.pdf

McSweeney et al. (2012, February 16). *UNDP Climate Change Country Profiles - Mozambique.* Retrieved February 7, 2016, from University of Oxford: http://www.geog.ox.ac.uk/research/climate/projects/undp-cp/UNDP_reports/Mozambique/Mozambique.hires.report.pdf

Mills-Gray, S. (1994, May 15). *Quality for Keeps: Drying Foods.* Retrieved from University of Missouri Extension: http://extension.missouri.edu/p/GH1562

PAEGC & TH Cologne. (2016). *Renewable Energy Resources and Technology Overview (Chapter B1)), Massive Open Online Course (MOOC).* Retrieved from Powering Agriculture - Sustainable Energy for Food: https://gc21.giz.de/ibt/var/app/wp385P/2624/wp-content/uploads/2015/03/PAEGC_MOOC_COMPILED_READER.pdf

Phinney et al. (2015). *Solar assisted pervaporation (SAP) for preserving and utilizing fruits in developing countries.* Kruger National Park, South Africa: Third Southern African Solar Energy Conference.

Piroschka Otte, P. (2014). *Solar cooking in Mozambique—an investigation of end-user's needs for the design of solar cookers.* Trondheim: Centre for Rural Research, University Centre.

Sekhar et al. (2009). Evaluation of Heat Loss Coefficients in Solar Flat Plate Collectors. *ARPN Journal of Engineering and Applied Sciences*, 15-19.

Tetra Pak. (1998). *The Orange Book.* Lund: Tetra Pak Processing Systems AB.

Tikekar et al. (2011). *Ascorbic acid degradation in a model apple juice system and in apple juice during ultraviolet processing and storage.* University park, USA: Dept of Food Science, the Pennsylvania State University.

Tokar, G. (1997). *Food drying in Bangladesh.* Dhaka: Agro-based industries and technology Project (ATDP).

UNDP. (2015). *Briefing note for countries on the 2015 Human Development Report, Mozambique.* New York: UNDP.

World Food Programme. (2016, February 20). *Mozambique.* Retrieved from World Food Programme: http://www.wfp.org/countries/mozambique

Yaldýz, O., & Ertekýn, C. (2001). Thin layer drying of some vegatables. *Drying Technology*, 583-597.

Appendix A

$$a_w = \frac{P_W}{P_{WS}} \tag{A}$$

$$G = \frac{G_{tot} \cdot \tau_{glass} \cdot \alpha_{abs}}{1 - R_{abs} \cdot R_{glass}} \tag{1}$$

$$h_{con,in} \cdot A_{abs} \cdot \left(\frac{T_{in} + T_{out}}{2} - T_{glass}\right) + h_{rad,in} \cdot A_{abs} \cdot (T_{abs} - T_{glass}) \tag{2}$$
$$- h_{con,out} \cdot A_{abs} \cdot (T_{glass} - T_{amb}) - h_{rad,out} \cdot A_{abs}$$
$$\cdot (T_{glass} - T_{sky}) = 0$$

$$h_{rad,in} = \frac{\frac{1}{\frac{1}{\varepsilon_{abs}} + \frac{1}{\varepsilon_{glass}} - 1} \cdot \sigma \cdot (T_{abs}^4 - T_{glass}^4)}{T_{abs} - T_{glass}} \tag{3}$$

$$h_{rad,out} = \frac{\varepsilon_{glass} \cdot \sigma \cdot (T_{glass}^4 - T_{sky}^4)}{T_{glass} - T_{sky}} \tag{4}$$

$$Nu = \frac{\left(\frac{f}{8}\right) \cdot (Re_{air} - 1000) \cdot Pr_{air}}{1 + 12{,}7 \cdot \left(\frac{f}{8}\right)^{\frac{1}{2}} \cdot (Pr_{air}^{\frac{2}{3}} - 1)} \tag{5}$$

$$f = (0{,}790 \cdot \ln(Re_{air}) - 1{,}64)^{-2} \tag{5}$$

$$Nu = \frac{h_{con,in} \cdot D_h}{\lambda_{air}} \tag{7}$$

$$D_h = \frac{2 \cdot Height \cdot Width}{Height + Width} \tag{8}$$

$$h_{con,in} \cdot A_{abs} \cdot \left(T_{abs} - \frac{T_{in} + T_{out}}{2}\right) + h_{con,in} \cdot A_{sides} \cdot \left(\frac{T_{abs} + T_{glass}}{2} - \right. \tag{9}$$
$$\left.\frac{T_{in} + T_{out}}{2}\right) - h_{con,in} \cdot A_{abs} \cdot \left(\frac{T_{in} + T_{out}}{2} - T_{glass}\right) - (T_{out} - T_{in}) \cdot X - (T_{out} -$$
$$T_{in}) \cdot C_{P,H2O} \cdot m_h - h_{con,out} \cdot A_{abs} \cdot (T_{glass} - T_{amb}) = 0$$

$$X = \rho_{air} \cdot C_{P,air} \cdot u_{air} \cdot A_{inlet} \tag{10}$$

$$\log(p_0) = A - \frac{B}{T + C} \tag{11}$$

$$RH = 100 \cdot \frac{P_w}{P_{ws}} \tag{12}$$

$$m_h = \frac{P_w}{R_V \cdot T_{amb}} \cdot A_{inlet} \cdot u_{air} \tag{13}$$

$$G - h_{con,in} \cdot \left(T_{abs} - \frac{T_{in} + T_{out}}{2}\right) - h_{rad,in} \cdot (T_{abs} - T_{glass}) - \frac{\lambda_{bottom}}{t_{bottom}} \tag{14}$$
$$\cdot (T_{abs} - T_{wall}) - \frac{\lambda_{side}}{t_{side}} \cdot \frac{A_{sides}}{A_{abs}} \cdot \left(\frac{T_{abs} + T_{glass}}{2} - T_{wall}\right)$$
$$- h_{con,in} \cdot \frac{A_{sides}}{A_{abs}} \cdot \left(\frac{T_{abs} + T_{glass}}{2} - \frac{T_{in} + T_{out}}{2}\right) = 0$$

$$h_{rad,in} = \frac{1}{\frac{1}{\varepsilon_{abs}} + \frac{1}{\varepsilon_{glass}} - 1} \cdot \sigma \cdot \frac{T_{abs}^4 - T_{glass}^4}{T_{abs} - T_{glass}} \tag{15}$$

$$\frac{\lambda_{bottom}}{t_{bottom}} \cdot (T_{abs} - T_{wall}) + \frac{\lambda_{side}}{t_{side}} \cdot \frac{A_{sides}}{A_{abs}} \cdot \left(\frac{T_{abs} + T_{glass}}{2} - T_{wall}\right) - h_{con,out} \tag{16}$$

$$\cdot \frac{(A_{abs} + A_{sides})}{A_{abs}} \cdot (T_{wall} - T_{amb}) - h_{rad,out1}$$

$$\cdot (T_{wall} - T_{amb}) - h_{rad,out1} \cdot \frac{A_{sides}}{2 \cdot A_{abs}} \cdot (T_{wall} - T_{amb})$$

$$- h_{rad,out2} \cdot \frac{A_{sides}}{2 \cdot A_{abs}} \cdot (T_{wall} - T_{sky}) = 0$$

$$h_{rad,out1} = \varepsilon_{wall} \cdot \sigma \cdot \frac{T_{wall}^4 - T_{amb}^4}{T_{wall} - T_{amb}} \tag{17}$$

$$h_{rad,out2} = \varepsilon_{wall} \cdot \sigma \cdot \frac{T_{wall}^4 - T_{sky}^4}{T_{wall} - T_{sky}} \tag{18}$$

$$h_{con,in} \cdot \left(\frac{T_{in} + T_{out}}{2} - T_{wall,in}\right) - \frac{\lambda_{dryer}}{t_{side}} \cdot (T_{wall,in} - T_{wall,out}) = 0 \tag{19}$$

$$\frac{\lambda_{dryer}}{t_{side}} \cdot (T_{wall,in} - T_{wall,out}) - h_{con,out} \cdot (T_{wall,out} - T_{amb}) - \frac{1}{2} \cdot h_{rad,out1} \tag{20}$$

$$\cdot (T_{wall,out} - T_{amb}) - \frac{1}{2} \cdot h_{rad,out2} \cdot (T_{wall,out} - T_{sky}) - z$$

$$= 0$$

$$(T_{in} - T_{out}) \cdot X - h_{con,in} \cdot A_{sides} \cdot \left(\frac{T_{in} + T_{out}}{2} - T_{wall,in}\right) + (T_{in} - T_{out}) \tag{21}$$

$$\cdot Cp_{H2O} \cdot m_h + \left(\frac{T_{in} + T_{out}}{2} - T_{out}\right) \cdot Cp_{H2O} \cdot m_{vap} - E_{vap}$$

$$= 0$$

$$E_{vap} = m_{vap} \cdot \Delta H_{vap,H2O} \tag{22}$$

$$m_{vap} = \frac{A_{bags}}{3600} \cdot (-1,0015 \cdot u_{bags} - 0,9565) \cdot RH + 0,3088 \cdot u_{bags} \tag{23}$$

$$+ 0,6297$$

Appendix B

Cross section	b/a	Nu (Uniform q_s)
	1,0	3,61
	1,43	3,73
	2,0	4,12
	3,0	4,79
	4,0	5,33
	8,0	6,49
	∞	8,23

48